Enhanced Evaluation of Hourly and Daily Extreme Precipitation in Norway from Convection-Permitting Models at Regional and Local Scales

Kun Xie[1,2], Lu Li[3], Hua Chen[1,2], Stephanie Mayer[3], Andreas Dobler[4], Chong-Yu Xu[5], Ozan Mert Göktürk[3]

[1]State Key Laboratory of Water Resources and Hydropower Engineering Science, Wuhan University, Wuhan

430072, P. R. China

[2]Hubei Provincial Key Lab of Water System Science for Sponge City Construction, Wuhan University, Wuhan, China

[3]NORCE Norwegian Research Centre, Bjerknes Centre for Climate Research, Bergen, Norway

[4]The Norwegian Meteorological Institute, Oslo, Norway

[5]Department of Geosciences, University of Oslo, P.O Box 1047 Blindern, 0316 Oslo, Norway

Correspondence to: Hua Chen (chua@whu.edu.cn); Lu Li (luli@norceresearch.no)

Abstract

Convection-permitting regional climate models (CPRCMs) have demonstrated enhanced capability in capturing extreme precipitation compared to regional climate models (RCMs) with convection-parameterization schemes. Despite this, a comprehensive understanding of their added values in daily or hourly extremes, especially at local scale, remains limited. In this study, we conduct a thorough comparison of daily and hourly extreme precipitation from the HARMONIE-Climate (HCLIM) model at 3 km resolution (HCLIM3) and 12 km resolution (HCLIM12) across Norway's diverse landscape, divided into five regions, using both gridded and in-situ observations. Our main focus is to investigate the added value of CPRCMs (i.e., HCLIM3) compared to RCMs (i.e., HCLIM12) for extreme precipitation from regional to local scales, and quantify to what extend CPRCMs can reproduce the orographic effect on extreme precipitation at both daily and hourly scales. We find that HCLIM3 better matches observations than HCLIM12 for daily and hourly extreme precipitation across most grid points in Norway, while HCLIM12 underestimates the extremes, especially for hourly extremes. At the regional scale, HCLIM3 captures the maximum 1-day precipitation (Rx1d) and maximum 1-hour precipitation (Rx1h) more accurately across most regions and seasons with some exceptions. Specifically, for daily extremes, it shows larger summer biases in the east, south and west, as well as return levels biases in the east; for hourly extremes, larger biases are observed in the summer and west, compared to HCLIM12. Besides, for local scale, HCLIM3 also outperforms HCLIM12 in most regions and seasons, except slightly larger summer bias of daily extreme in the south and west. Overall, HCLIM3 consistently

33   demonstrates added value in simulating daily extremes in the middle and north regions at both regional and local

34   scales, as well as hourly extremes at all 10 stations, compared with HCLIM12. Both HCLIM3 and HCLIM12

35   capture the seasonality of daily extremes well, while HCLIM3 performs better for the hourly extremes, accurately

36   representing their frequency and intensity. Additionally, both models capture the reverse orographic effect of Rx1h

37   at the regional scale with no added value seen in HCLIM3, while at local scale, HCLIM3 shows added value

38   compared to HCLIM12 in representing the reverse orographic effect of Rx1d in all seasons except summer. This

39   study highlights the importance of more realistic CPRCMs in providing reliable insights into the characteristics of

40   precipitation extremes across Norway's five regions. Such information is crucial for effective adaptation

41   management to mitigate severe hydro-meteorological hazards, especially for the local extremes.

42   **1 Introduction**

43   In recent years, the world has witnessed a surge in both frequency and intensity of floods primarily attributed to the

44   increasing occurrence of intensive rainfall events (Tabari, 2020). These changes underscore the pressing need to

45   develop a predictive understanding of precipitation extremes for the upcoming decades, given the ongoing globe

46   warming. The intensification of precipitation extremes under the influence of global warming has the potential to

47   trigger severe natural hazards and exert significant socioeconomic impacts (Thackeray et al., 2022), which has

48   gained substantial attention in recent research endeavors. However, most previous research in this field relied on

49   coarse-resolution GCMs with grid sizes exceeding 100 km, which struggle to accurately simulate extreme

50   precipitation events and their frequency due to the limitations of their coarser resolution (Piani et al., 2010; Wang et

51   al., 2017). Notably, these GCMs tend to produce the largest errors in predicting extreme precipitation, particularly in

52   cases involving heavier convective activity, as observed in the study by Gervais et al. (2014a). Despite various bias-

53   correction techniques are applied to mitigate these discrepancies on the GCMs, as well as employing them as forcing

54   data for regional climate models (RCMs) with grid size larger than 10 km, it remains a persistent challenge to

55   eliminate the transfer of biases from GCMs to RCMs, as noted by studies such as Pontoppidan et al. (2018) and Kim

56   et al. (2020). The large resolution gap between GCMs or RCMs and localized precipitation extremes further

57   constrains the robust simulations of extreme precipitation as highlighted by Li et al. (2020a). In addition, the

58   reliance on parameterization schemes to represent convection in these coarse resolution models introduces a

59   significant source of uncertainty in modelling errors (Prein et al., 2015; Kendon et al., 2019). More frequent and

60   intense precipitation events under global warming stimulate interest in higher resolution and physics-based models

61   to improve the estimation of short-duration extremes.

62   Convection-permitting regional climate models (CPRCMs), with grid size of less than 4 km, offer a promising

63   alternative, which explicitly represent convection, eliminating the need for parameterizations of deep atmospheric

64   convection. The potential in resolving deep convection and local extremes from CPRCMs lead to the realistic

65   representation in daily and sub-daily precipitation features, including diurnal cycle, intensity and frequency of heavy

66   precipitation events, seasonality, spatial-temporal pattern, wet-spell and dry-spell. For instance, CPRCMs have been

67   proven to reduce the bias and enhance the representation in precipitation intensity and intensity in the Tibetan

68 Plateau, the highest highland in the world, as shown in Li et al. (2021). In addition to their capability in capturing

69 precipitation, Liu et al. (2017) also demonstrated the confidence of CPRCMs in estimating snowfall and snowpack

70 in the central U.S. Furthermore, the importance of CPRCMs in representing dry spell, dry and wet extremes induced

71 by local convective activity across Africa has also been found in Kendon et al. (2019), Chapman et al. (2023) further

72 confirmed its benefit in capturing rare rainfall extreme and local feature. In UK, Kendon et al. (2023) and Kent et al.

73 (2022) have found the benefit of CPRCMs compared to RCMs with convection parameterization schemes.

74 Additionally, the superior performance in capturing hourly and daily extreme precipitation including return-level,

75 frequency and intensity from CPRCMs over Alpine in Europe, has also been highlighted by Adinolfi et al. (2021),

76 Dallan et al. (2023) and Giordani et al. (2023).

77 Northern Europe has been reported to experience a strong increase in precipitation, as indicated by Dyrrdal et

78 al., (2023). Thus, a novel CPRCM has been developed within the Nordic Convection Permitting Climate Projections

79 project (NorCP) based on the HARMONIE-Climate model (HCLIM), cycle 38 (HCLIM38; Belušić et al., 2020) and

80 applied at a resolution of 3 km (HCLIM3). To investigate the added value of the convection-permitting resolution,

81 HCLIM38 has also been run at a (not convection-permitting) resolution of 12 km (HCLIM12). For convenience,

82 HCLIM3 and HCLIM12 are used in the following to represent the HCLIM38 simulations at the two resolutions, i.e.

83 the CPRCM and ordinary RCM, respectively. The term HCLIMs indicates the two of them, HCLIM3 and

84 HCLIM12.

85 Through comparisons of seasonal precipitation, daily mean precipitation, higher-intensity daily precipitation,

86 the diurnal of hourly precipitation including frequency and intensity from HCLIM3 and HCLIM12 over Fenno-

87 Scandinavia, Lind et al. (2020) emphasized the added value of CPRCMs in reproducing extreme precipitation,

88 primarily over complex terrain, compared to a coarser-scale model. Médus et al. (2022) also noted that the summer

89 diurnal cycle of frequency and intensity of hourly precipitation was correctly captured in HCLIM3 compared to

90 HCLIM12 in the Nordic region, with HCLIM12 underestimating the diurnal cycle. However, the evaluation and

91 conclusions from Lind et al. (2020) and Médus et al. (2022) mainly focused on the large regional and country scale

92 of Fenno-Scandinavia, overlooking the added values of CPRCMs at local scale. Furthermore, Thomassen et al.

93 (2023) observed that HCLIM3 tends to exhibit underestimations in monthly precipitation and a later evening peak

94 compared to sub-kilometre models. They found that the advantages of sub-kilometer models were not outstanding.

95 These evaluations were based on gridded datasets, which introduce uncertainty at the local scale, especially over

96 complex orography (Lussana et al., 2019). As Chapman et al. (2023) demonstrated, who underscored the importance

97 of assessing rare extreme rainfall events in eastern African using convection-permitting models and parameterization

98 convection models at both grid and station scales, the extreme from grids representing rainfall averaged over a larger

99 area are damped and hence the return-level will be smaller than observation. They found that the station-derived

100 shape parameters and return levels are aligned with observations and suggested the significance of site-specific

101 analysis and evaluations. The error induced by station density in gridded dataset has also been indicated in Gervais

102 et al. (2014b), who suggested the source of large errors in gridded dataset when station density is low. Consequently,

103   a comprehensive evaluation and analysis of the added value from CPRCMs compared with RCMs that incorporates

104   both regional and local scales is crucial for extreme precipitations.

105   We acknowledge that Norway, a Nordic country, is representative of diverse climate features due to its

106   extended latitude, rugged coastline, plateaus, and complex orography. The dominances of precipitation between the

107   coastal and inland regions over Norway are distinctly different, and most of studies focusing on the hydrology and

108   meteorology over Norway were based on the divided regions (Vormoor et al., 2016; Poujol et al., 2021; Konstali

109   and Sorteberg, 2022). By dividing region with its characteristics, a more thorough comprehension of added value of

110   CPRCMs in capturing extreme precipitation can be reached. Therefore, reliable evaluation about analyzing the adder

111   value of CPRCMs in capturing extreme precipitation should be scaled to region or local scale.

112   In the complex mountain areas, extreme precipitation is triggered by the interaction of large-scale atmospheric

113   activity and local orography property, which may cause severe hydrometeorological hazards, such as flash flooding.

114   However, understanding the orographic impact in precipitation in complex orography is challenging due to sparse

115   observations (Rossi et al., 2020). The poor representation of RCMs in capturing local precipitation have been

116   indicated in Knist et al. (2020). Importantly, CPRCMs shows advantage in reproducing precipitation bias over

117   higher complex orography in the Alpine, as shown in Lind et al. (2016) and Reder at al. (2020). Furthermore, the

118   better representation of sub-daily and daily heavy precipitation from CPRCMs over the Alpine have also been found

119   in Ban et al. (2020) and Dallan et al. (2023). Marra et al. (2021) and Dallan et al. (2023) also confirmed the

120   efficiency of CPRCMs in reproducing the reverse orography effect on hourly extreme precipitation. The relationship

121   between extreme precipitation and elevation may vary depending on latitude and climate zones (Amponsah et al.,

122   2022). Rossi et al. (2020) and Mahoney et al. (2015) found the weak depend of sub-daily precipitation on elevation

123   in Colorado, USA. Opposing the orographic enhance on daily precipitation, Dallan et al. (2023) indicated the no

124   evident relation of daily precipitation on elevation. It is worth noting that the potential added value of CPRCMs in

125   representing orographic effects compared to RCMs has not been explored. Moreover, the performance of CPRCMs

126   varies with seasons, which underscores the need to explore the orographic effects on seasonal extremes. Thus, we

127   fill this knowledge gap by characterizing orographic impact on hourly and daily extreme precipitation seasonally.

128   As highlighted by Konstali and Sorteberg (2022), there can be significant uncertainties associated with the

129   interpolation of grided precipitation data. Besides, the benefit for precipitation spatial evaluation based on in-situ

130   observation has also been reported in Thomassen et al. (2023). Therefore, the evaluation of extreme precipitation

131   from HCLIM3 and HCLIM12 here, is based on both gridded precipitation and in-situ observation. Our study aims to

132   address the value of CPRCMs (HCLIM3) in capturing the characteristics of extreme precipitation in Norway,

133   comparing it with a coarser resolution model (HCLIM12) as well as both of the in-situ and gridded precipitation

134   observations. Here, our contribution to the existing literature, e.g., Médus et al. (2022), revolves around the added

135   value of CPRCMs in the extreme precipitation characteristics, encompassing a range of metrics.

136   The main objectives of this study are to: (1) enhance the understanding of convection-permitting climate

137   models and highlighting the added value of CPRCMs by comparing their effectiveness in simulating extreme

138 precipitation with that of regional climate models from regional to local scales; (2) assess HCLIM3's capability in

139 depicting orographic effects on seasonal extreme precipitation. This research explores whether the benefits provided

140 by CPRCMs are consistent in different regions driven by varying physical processes for precipitation. Finally, our

141 study delves into the analysis of the intensity and frequency of extreme precipitation events, offering insights into

142 local and regional variations.

143 **2 Study area and data**

144 **2.1 Study area**

145
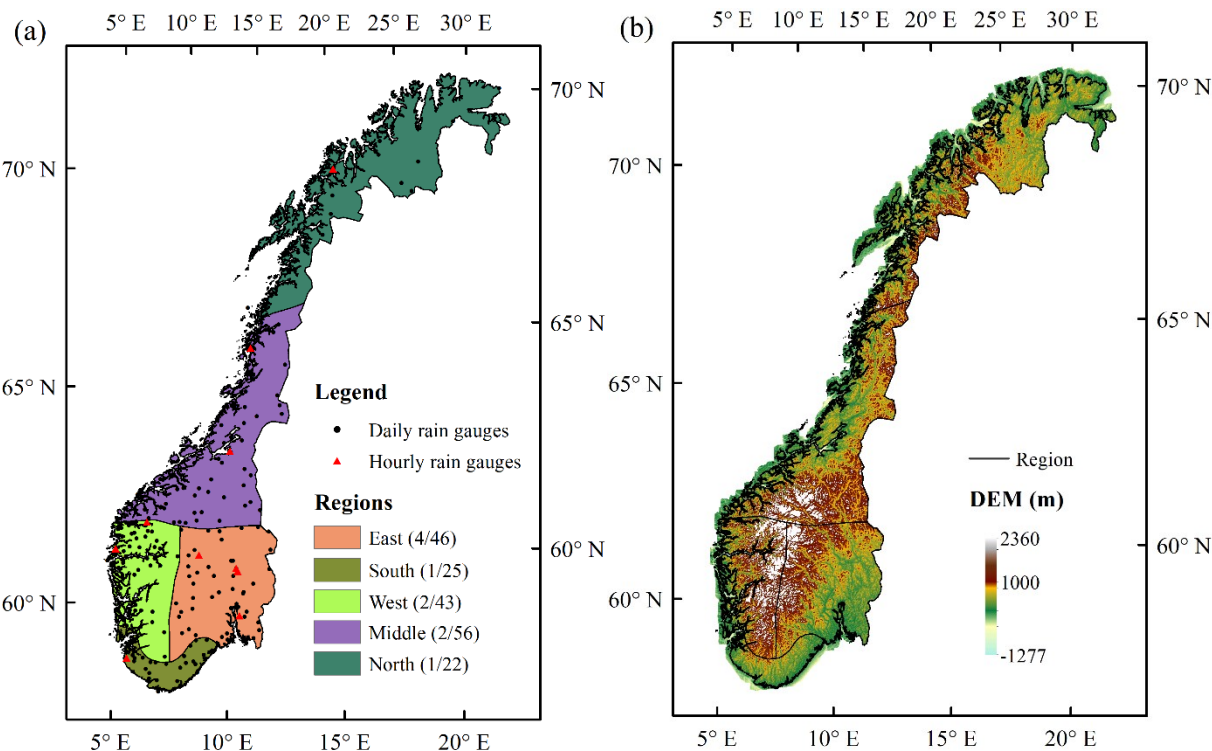
146 **Figure 1: (a) The division of five regions in Norway. In the legend, the numbers shown in the brackets after each region**
147 **represent the available size of hourly / daily stations in the region during 1999 – 2018. For example, East (4/46) means**
148 **that there are available data from 4 hourly stations and 46 daily stations in the East during 1999-2018; (b) Spatial**
149 **distribution of topography over Norway.**

150

151 The different climate regimes between coastal and inland regions over Norway compels the analysis of hydro-

152 meteorology based on divided regions. Based on similar seasonal cycle characteristics, Michel et al. (2021) and

153 Konstali and Sorteberg (2022) divided the Norwegian continent into eight regions. Taking into account the spatial

154 distribution of rain gauges and ensuring that each region has at least one hourly rain-gauge, we combined the south

155 and southwest into the south, and the middle-inland and north into the north. Therefore, mainland Norway in this

156 study is divided into five regions: East (E), South (S), West (W), Middle (M), and North (N), as shown in Fig. 1.

157 The study areas cover the mainland Norway which has unique climate characteristics within different regions.

158 Precipitation in Norway primarily occurs along the coast in late autumn and winter, while inland areas receive more

159 precipitation in summer. The east region with stratiform precipitation originating from south is dominant by

160 continental climate, with convective precipitation in summer. The west coast of Norway is strongly affected by the

161 North Atlantic storm track, where precipitation from frontal systems and landfalling storms is enhanced due to the

162 orographic uplift over Scandinavia (Poujol et al., 2021). Most extreme events occurring in the west region with

163 abrupt topography, are mainly related to atmospheric rivers (AR), which are generally linked to extratropical

164 cyclones during cooler seasons (Whan et al., 2020). Additionally, in the summer, AR coincides with more frequent

165 convective activities (Poujol et al., 2021). The south region lies at the end of the climatological jet and is regularly

166 affected by the AR especially during the Zonal and Atlantic trough weather regimes (Michel et al., 2021), while

167 convective activities play a crucial role in the south regions in summer (Li et al., 2020b). For the middle and north

168 regions, 59% of extremes are associated with AR, and the precipitation rate decreases moving inland (Konstali and

169 Sorteberg, 2022).

170 **2.2 Data**

171 We utilize the outputs of double nested model simulations from the HCLIM38 model, which include different

172 configuration settings for each spatial resolution: HCLIM3 and HCLIM12. HCLIM12 covers most of Europe with

173 313 ×349 grid-points using the ERA-Interim reanalysis (~80 km) as the boundary condition, and HCLIM3 spans the

174 Fenno-Scandinavia region with 637×853 grid-points using the output of the HCLIM12 as the boundary condition for

175 every 3 h. Importantly, the convection-parameterization scheme was switched-off in HCLIM3, allowing for an

176 explicit representation of convection processes. The present-day simulations from HCLIM3 and HCLIM12 span the

177 years 1997-2018. For more comprehensive information, refer to the work of Lind et al. (2020) and Médus et al.

178 (2022).

179   This study primarily focuses on assessing the performance of HCLIM3 and HCLIM12 in simulating hourly

180 and daily extreme precipitation events in mainland Norway for the present-day period (1997-2018, with the first two

181 years excluded). The model outputs from HCLIM3 and HCLIM12 are specifically extracted for mainland Norway.

182 Before analysis, HCLIM3 data was remapped to the HCLIM12 grid (12km) using a bilinear interpolation method.

183   Precipitation from the seNorge2018 (SeNorge) gridded dataset, covering Norway with 1-day temporal and 1

184 km spatial resolution since 1957 (Lussana et al., 2019), is used as the observation dataset to evaluate the

185 performance of HCLIM3 and HCLIM12 during 1999-2018. Precipitation from the SeNorge2 gridded dataset, with

186 1-hour temporal and 1 km spatial resolution, is also applied to evaluate the hourly result during 2010-2018 (Lussana

187 et al., 2018). In addition, in-situ precipitation of observations, including both 1-hour and 1-day resolutions, are

188 downloaded from Norwegian Meteorological Institute Frost API (met.no).

189 **3 Methods**

190 **3.1 Evaluation of precipitation**

191 To evaluate the characteristics of precipitation extremes between HCLIM3 and HCLIM12, we compared the

192 historical simulations with daily SeNorge gridded dataset, hourly SeNorge2 gridded dataset and in-situ observations.

193 We only keep the stations that have less than 10% of the data missing during 1999-2018 and consider station

194 distribution uniformity, which give a total of 192 daily stations and 10 hourly stations, respectively, over Norway

195 (Fig. 1, Table S1 and Table S2). In this study, the evaluation based on in-situ observation and gridded dataset

196 (SeNorge and SeNorge2) was defined as the local scale and regional scale, respectively.

197   Remapping finer-resolution data to a coarser resolution reduces the influence of such artifacts by averaging out

198 the variability. This approach is consistent with the methodology used by Lind et al. (2020) and Médus et al. (2022),

199 who also remapped all data to a coarser grid when comparing the performance of HCLIM3 and HCLIM12. Lind et

200 al. (2020) observed that the differences between HCLIM3 data remapped to the coarser native grid of HCLIM3 and

201 the HCLIM12 grid were minimal. Importantly, they found that the improvements of HCLIM3 persisted even after

202 spatial aggregation, indicating that the enhanced resolution of the model offered benefits that were preserved when

203 viewed on a coarser grid. Therefore, HCLIM3, SeNorge and SeNorge2 were remapped to HCLIM12 grid~12 km for

204 the evaluation at regional scale. For the SeNorge and SeNorge2 based assessments, the extreme indices are first

205 calculated at the grid-point level and then the regional averages are computed. For the evaluation based on in-situ

206 observation, HCLIM3 and HCLIM12 were interpolated to the 192 daily rain-gauges and 10 hourly rain-gauges to

207 calculate the indices using bilinear interpolation method.

208   For the evaluation of extreme precipitation, we examined the maximum 1-day precipitation (Rx1d), maximum

209 1-hour precipitation (Rx1h), return-period-based precipitation amounts at 5, 10, 20, and 50-year return periods, and

210 seasonality of frequency/intensity from regional to local scales. The calculation of seasonal Rx1d/Rx1h was based

211 on the maximum value within one season per year.

212 **3.2 Extreme precipitation indices**

213 The Generalized Extreme Value (GEV) distribution was used to estimate precipitation intensity for specific return

214 periods (e.g., 5, 10, 20, and 50 years). The return levels were calculated by fitting the annual maximum discharge

215 derived from observed and simulated daily data (both gridded and rain gauges), and hourly data (only 10 rain

216 gauges), to GEV distribution. Then, the quantile Z_p of the GEV distribution with a return period of $\frac{1}{p}$ can be

217 obtained. GEV distribution has been widely used to model extreme events in meteorology (Coles et al., 2003). The

218 cumulative distribution function $F(x)$ and probability density function $f(x)$ of GEV were as follows to calculate the

219 return level Z_p:

220

221 $$F(x) = exp\left\{-\left[1 - k\left(\frac{x-\xi}{\alpha}\right)\right]^{1/k}\right\}, k \neq 0 \tag{1}$$

222 $$f(x) = \frac{1}{\alpha}\left[1 - k\left(\frac{x-\xi}{\alpha}\right)\right]^{1/k-1} exp\left\{-\left[1 - k\left(\frac{x-\xi}{\alpha}\right)\right]^{1/k}\right\} \tag{2}$$

223 $$Z_p = \xi - \frac{\alpha}{k}\left\{1 - [-log(1-p)]^{-k}\right\} \tag{3}$$

224

225   Where, α, ξ, and k indicates the scale, location and shape parameter, respectively. Kolmogorov-Smirnovs,

226 Anderson-Darlings, and Chi-Square tests were performed to determine if the GEV was accepted to fit the maxima

227 series.

228

3.3 Quantification of the orographic effect

230 The orographic effect on Rx1h and Rx1d precipitation was explored by looking at the relationship with elevation of
231 the annual and seasonal maxima from regional to local scales. A linear regression model (Di Piazza et al., 2011) was
232 utilized to approximate the relations. The relationship of elevation with observation (Rx1h: SeNorge2; Rx1d:
233 SeNorge and daily in-situ observation) and simulation (HCLIM3 and HCLIM12) was fitted to compute the linear
234 regression slope. To eliminate the impact of unit (Rx1h and Rx1d), the slope is converted to a relative slope with
235 respect to the average value of extreme precipitation, expressed as percentage precipitation (%) per kilometer of
236 elevation. This is done by dividing the mean extreme precipitation value for the entire study region computed
237 separately for daily and hourly extremes. The orographic effect at local scale was only based on daily in-situ
238 observation due to the limited hourly in-situ observation. At local scale, the elevation for each rain-gauges was
239 extracted according to the digital elevation model. At regional scale, the grid of digital elevation model and
240 HCLIM3 was resample to the same grid resolution of 12 km as HCLIM12 before calculation. Only the grids and
241 stations above sea level of 0 m are included to quantify the orographic effect.
242 If the precipitation increases with elevation, there is an orographic effect on extreme precipitation; if the
243 precipitation decreases with elevation, this means a reverse orographic effect on extreme precipitation.

4 Results

4.1 Evaluation of daily extreme with SeNorge

4.1.1 Maximum 1-day precipitation (Rx1d)

247 Figure 2 provides a comprehensive comparison of percentage biases of Rx1d from HCLIM3 and HCLMI12
248 compared to SeNorge. From Fig. 2 (a), we can see that HCLIM12 has more grids with underestimated Rx1d than
249 HCLMI3 in Norway, which is confirmed clearly in Fig. 2 (b) showing density plot of the percentage bias
250 distribution from two models compared with SeNorge. Specifically, more grids from HCLIM3 than HCLIM12 tend
251 to overestimate Rx1d within the 0-25 % range, while HCLIM12 leans towards larger underestimation within the -
252 10-50%. The density curve in Fig. 2 (b) reflects a higher peak at 0 for HCLIM3, indicating a more accurate
253 representation of Rx1d with an average dry-bias with 1.6%. Conversely, HCLIM12 shows a 7% dry-bias for Rx1d
254 on average.
255 Figure 2 (c) shows the absolute percentage bias of annual and seasonal Rx1d from HCLIM3 and HCLIM12
256 compared to SeNorge for five regions in four seasons. In annual, HCLIM3 exhibit added value in capturing annual
257 Rx1h in the five regions compared to HCLIM12. HCLIM3 better captures Rx1d in four seasons and annual for five
258 regions than HCLIM12, while HCLIM12 shows larger bias in most regions except in the east, south and west during
259 summer. In summer, HCLIM3 only outperforms Rx1d in the middle and north over HCLIM12. Overall, HCLIM3
260 shows notably added value in Rx1d comparing with HCLMI12 across regions and seasons except in summer.

261
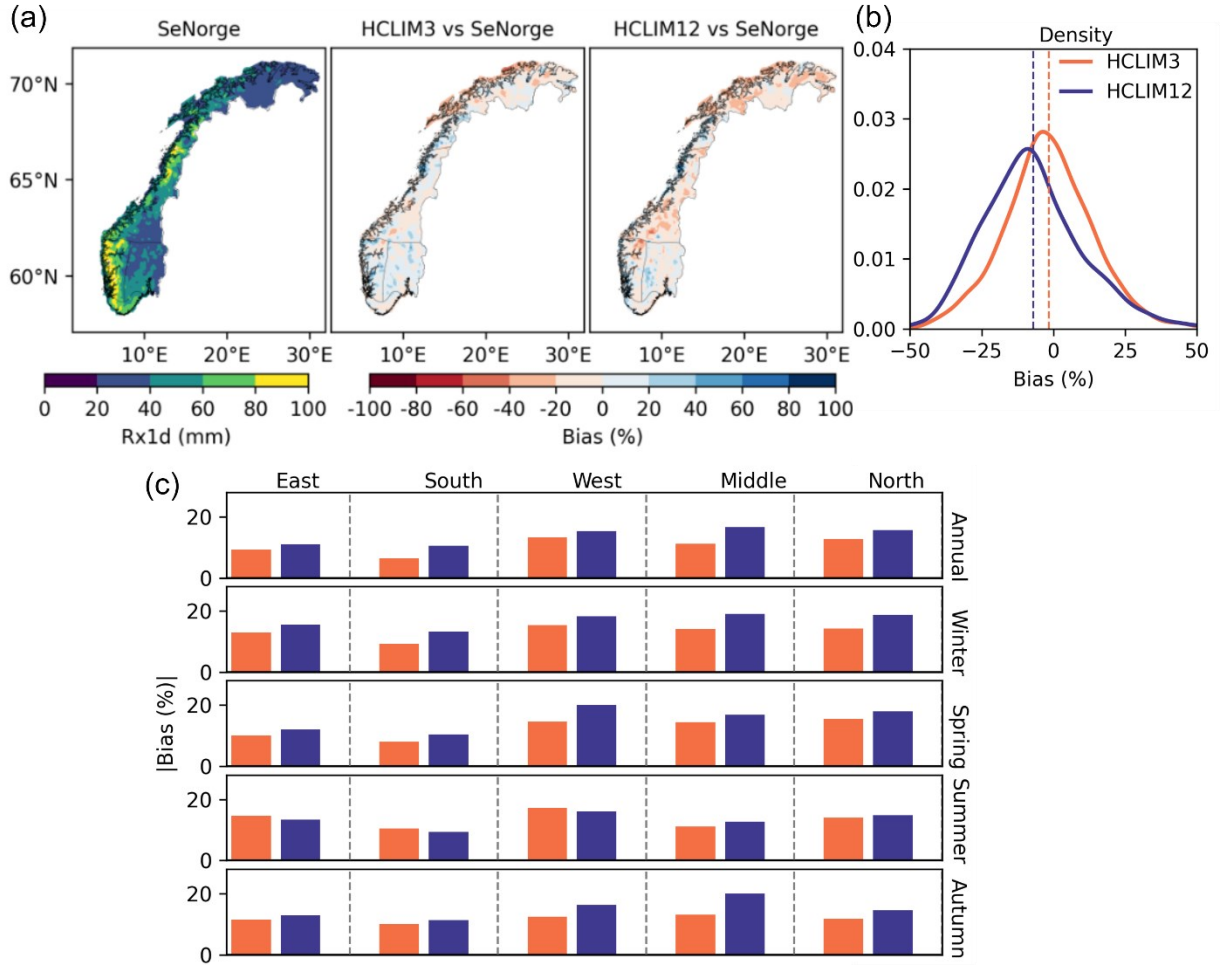
Figure 2: (a) The annual Rx1d of SeNorge, and the percentage bias of Rx1d from HCLIM3 and HCLIM12 to SeNorge during 1999-2018; (b) density plot of the percentage bias distribution for annual Rx1d from HCLIM3 and HCLIM12 compared to SeNorge for Rx1d during 1999-2018 (The dashed lines represent the mean bias); (c) the absolute percentage bias of annual and seasonal Rx1d from HCLIM3 and HCLIM12 to SeNorge for five regions. The bias is first calculated at the grid-point level, and then regional averages are computed. For (a) and (b), the percentage bias is equal to model simulations minus observations, divided by observations. For (c), the absolute percentage bias is calculated as the absolute difference between simulations and observations, divided by observations.

Furthermore, as shown in Fig. 3, a comparison of the Rx1h percentage biases of HCLIM3 and HCLIM12 with SeNorge2 for the period 2010-2018 demonstrates that HCLIM3 has a clearly added value in simulating the annual Rx1h in Norway, with smaller wet biases on average, while HCLIM12 shows larger dry biases over the whole of mainland Norway. At the regional scale, HCLIM3 also shows added value in capturing annual and seasonal Rx1h than HCLIM12 in five regions except west and middle regions. Specifically, in the west region, HCLIM3 exhibits larger absolute percentage biases than HCLIM12 in annual Rx1h and seasonal Rx1h than HCLIM12, except in spring. In summer, only in the south and north regions, the Rx1h bias of HCLIM3 is smaller than that of HCLIM12.
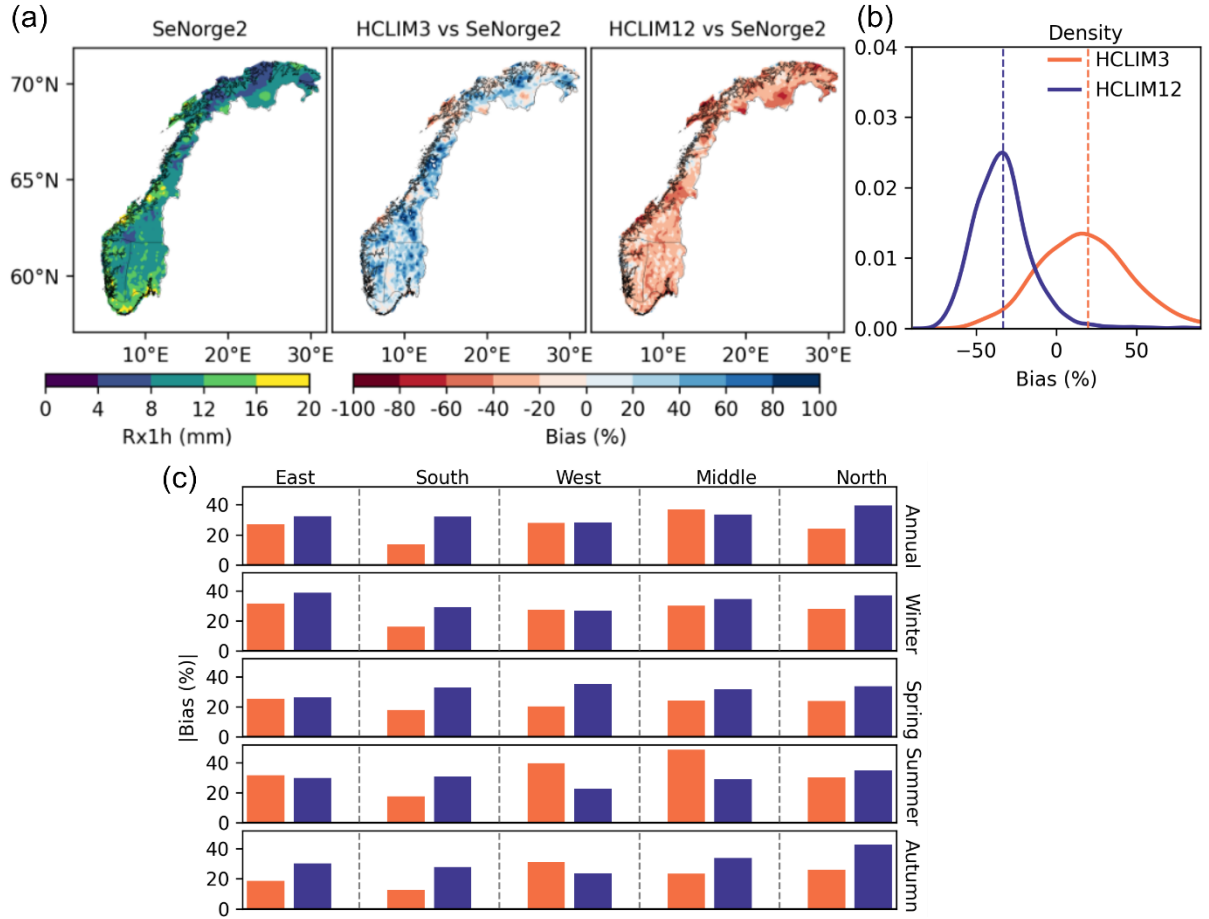
Figure 3: (a) The annual Rx1h of SeNorge2, and the percentage bias of Rx1h from HCLIM3 and HCLIM12 to SeNorge2 during 2010-2018; (b) density plot of percentage bias for annual Rx1h distribution from HCLIM3 and HCLIM12 compared to SeNorge2 during 2010-2018 (The dashed lines represent the mean bias); (c) the absolute percentage bias of seasonal Rx1h from HCLIM3 and HCLIM12 to SeNorge2 for five regions. For (a) and (b), the percentage bias is equal to model simulations minus observations, divided by observations. For (c), the absolute percentage bias is calculated as the absolute difference between simulations and observations, divided by observations.

4.1.2 Return levels

Figure 4 shows the bias in estimated daily precipitation for 5-, 10-, 20-, and 50-year return periods during 1999-2018 across five regions (compared to SeNorge). The great interregional variation is shown between HCLIM3 and HCLIM12. Relative to SeNorge, HCLIM3 tends to overestimate return-levels in the east and west regions, while underestimates them in the others. By comparison, except for the east region where HCLIM12 shows overestimation, the extreme precipitation estimates in most other regions are underestimated. The performance of HCLIM3 in capturing extremes varies across regions. HCLIM3 and HCLIM12 exhibit percentage biases of opposite sign in simulating return level precipitation in the west region, where HCLIM3 overestimates and HCLIM12 underestimates precipitation at different return periods. In the west, middle, and north regions, HCLIM3 outperforms HCLIM12 in all return periods, but the performance is less satisfactory in the east region.

296   Given the societal impacts of precipitation extremes, understanding how HCLIM3 and HCLIM12 represent
297   these extremes is crucial. The physical processes driving precipitation in inland and coastal regions, as highlighted
298   by Konstali and Sorteberg (2022), emphasize the need for a separate evaluation for each region with different
299   characteristics. This approach ensures a more robust assessment, providing valuable information for regional
300   authorities.
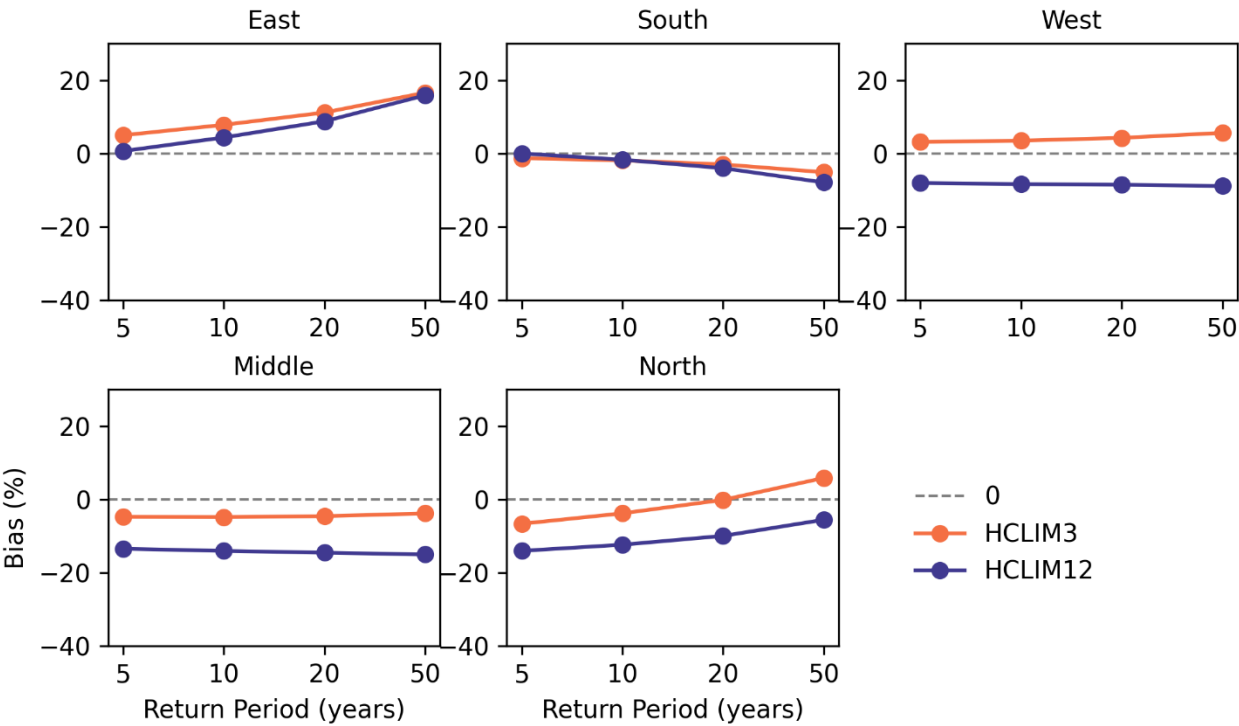
301
302 **Figure 4: Percentage bias of extreme daily precipitation exceeding the 5-year to 50-year return periods over five regions**
303 **between SeNorge and HCLIMs (i.e., HCLIM3 and HCLIM12). Return periods of 5-, 10-, 20-, and 50-year are calculated**
304 **on the basis of GEV.**

4.2 Evaluation of daily extreme with in-situ data

4.2.1 Maximum 1-day precipitation (Rx1d)
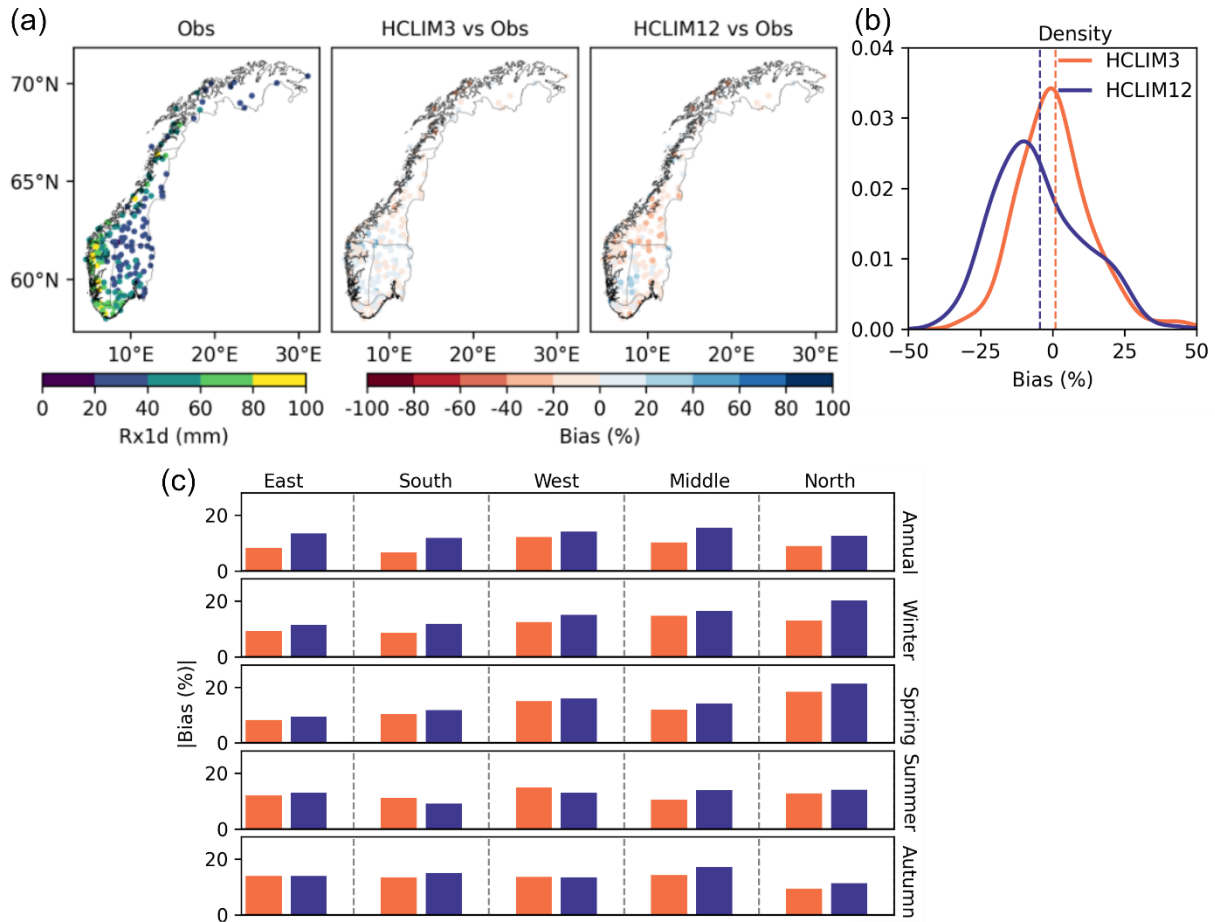
Figure 5: (a) The annual Rx1d of in-situ observation, and the percentage bias of Rx1d from HCLIM3 and HCLIM12 to in-situ observation during 1999-2018 over 194 stations; (b) density distribution of percentage bias for annual Rx1d between HCLIMs and observations from 194 stations during 1999-2018 (The dashed lines represent the mean bias); (c) the absolute percentage bias of seasonal Rx1d between HCLIMs and observations across the five regions. For (a) and (b), the percentage bias is equal to model simulations minus observations, divided by observations. For (c), the absolute percentage bias is calculated as the absolute difference between simulations and observations, divided by observations.

Similar to the regional results in Fig. 2, Fig. 5 shows the percentage bias of annual and seasonal Rx1d from HCLIM3 and HCLIM12 in comparison to in-situ observations. Notably, a difference between HCLIM3 and HCLIM12 can be seen at local scale compared to regional result: a greater number of sites from HCLIM3 approach zero-bias, and more grids from HCLIM12 shows a dry bias about 10-40%, as shown in Fig. 5 (b). On average, HCLIM12 with 4.5% dry-bias tends to underestimate annual Rx1d, while HCLIM3 represents added value in capturing annual Rx1d with 1% wet-bias on average at local scale. Furthermore, HCLIM3 shows added value in simulating the annual Rx1h at local scale in all regions.

From a seasonal perspective, as shown in Fig. 5 (c), overall, HCLIM3 shows added value in capturing the seasonal Rx1d in most regions and seasons, except for summer. Specifically, HCLIM3 performs better than

324   HCLIM12, except for the west and south region, where HCLIM3 exhibits a larger bias in summer Rx1d. In

325   particular, the added value of HCLIM3 in simulating autumn Rx1d in the east and west is not as obvious when

326   compared to HCLIM12.

327   It is noteworthy that at the local scale, HCLIM3 and HCLIM12 perform similarly to the regional results in most

328   regions. There are some exceptions, such as, HCLIM3 shows larger biases in summer Rx1d in the south and west

329   compared with HCLIM12 at both regional and local scales. In contrast to the clearly larger bias in Rx1h at the

330   regional scale for both HCLIM3 and HCLIM12, a relatively smaller bias in Rx1d is demonstrated at both regional

331   and local scales. At the regional scale, HCLIM3 exhibits added value in all seasons except summer, while at the

332   local scale, HCLIM3 and HCLIM12 show similar biases in autumn Rx1d in the east and west, which means that the

333   advantage of HCLIM3 over HCLIM12 at the local scale in autumn weakens in the west and east compared with the

334   regional scale.

335   **4.2.2 Return-levels**
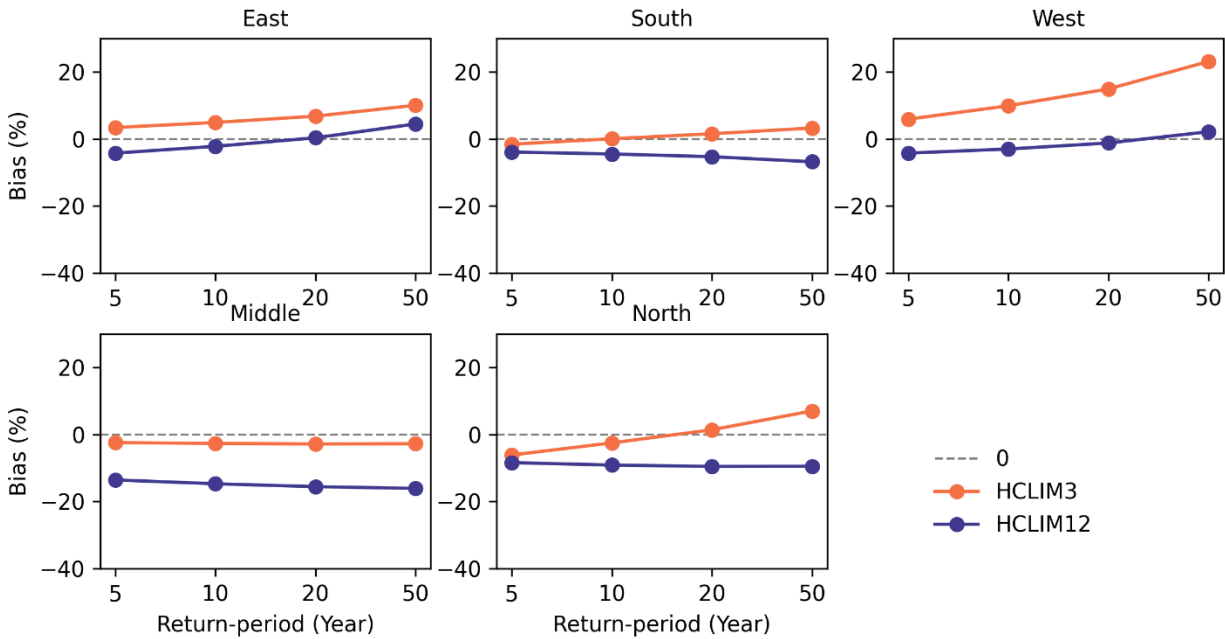
337   **Figure 6: Percentage bias of extreme daily precipitation exceeding the 5-year to 50-year return periods over five regions**
338   **between HCLIMs (i.e., HCLIM3 and HCLIM12) and in-situ observation in the 192 daily rain-gauges. Return periods of**
339   **5-, 10-, 20-, and 50-year are calculated on the basis of station-scale GEV.**

341   Figure 6 shows the percentage bias of the estimated daily return levels (e.g., 5-, 10-, 20-, and 50-year return periods)

342   from HCLIM3 and HCLIM12 compared to observations for the period 1999-2018. The figure illustrates the average

343   bias of return-levels for the stations in the corresponding regions. Compared with the in-situ observation, HCLIM3

344   overestimates the return levels in the east and west for all return periods (5-, 10-, 20-, and 50-year) and

345   underestimates return levels in the south and north for 20- and 5-year return periods, while HCLIM12

346   underestimates the return levels in all regions. Generally, HCLIM3 can more accurately represent the return levels in

347   most regions compared to HCLIM12. The biases of HCLIM3 and HCLIM12 vary across regions and return periods.

348 HCLIM3 has lower biases than HCLIM12 in most regions, except for the east and west regions. Both HCLIM3 and
349 HCLIM12 perform well in the south region. In addition, Fig. S1 shows the range of the return levels for all stations
350 in the corresponding region, and HCLIM3 introduces larger variations in the west and south regions compared with
351 HCLIM12, as indicated by the wider whiskers.

4.3 Evaluation of hourly extreme with in-situ data

4.3.1 Maximum 1-hour precipitation (Rx1h)

354 The time evolution of annual Rx1h from HCLIM3 and HCLIM12 is compared to in-situ observation during 1999-
355 2018, as shown in Fig. 7. Compared to HCLIM12, HCLIM3 shows distinct superior in capturing the time evolution
356 of annual Rx1h, even with underestimation and time shifting at some local places. For example, the annual Rx1h
357 above 25 mm/hour at Kvithamar (SN69150), Særheim (SN44300), Tromsø - Holt (SN90400), Tjøtta (SN76530) and
358 Løken i Volbu (SN23500) is struggle to be captured by HCLIM3 and HCLIM12. However, HCLIM3 well capture
359 the annual Rx1h in other local places, despite of the time deviation of annual Rx1h. Taking the site Østre Toten -
360 Apelsvoll (SN11500) as an example to illustrate the time deviation: HCLIM3 simulate that the annual Rx1h (37
361 mm) in the past 20 years was in 2001, four years earlier than the in-situ observation (35 mm). Furthermore, to better
362 assess the annual variability of Rx1h, we extracted grids within a 12 km radius of each station and calculate the
363 uncertainty range (Fig. S2), which reveals that the interpolated local Rx1h precipitation from HCLIM12, particularly
364 over grids with a larger area, tends to be damped, resulting in a narrower range than HCLIM3. Based on station
365 statistics of annual mean Rx1h in Norway, the boxplot (Fig. 7) shows that the annual mean Rx1h of HCLIM3 is
366 within the range of observed values. In contrast, HCLIM12 consistently underestimates Rx1h, with all its values
367 being below the observed minimum. Despite outperforming than HCLIM12, it is noteworthy that HCLIM3
368 demonstrates limitations in reproducing the accurate occurrence time and magnitude of annual Rx1h at local-level in
369 Norway.
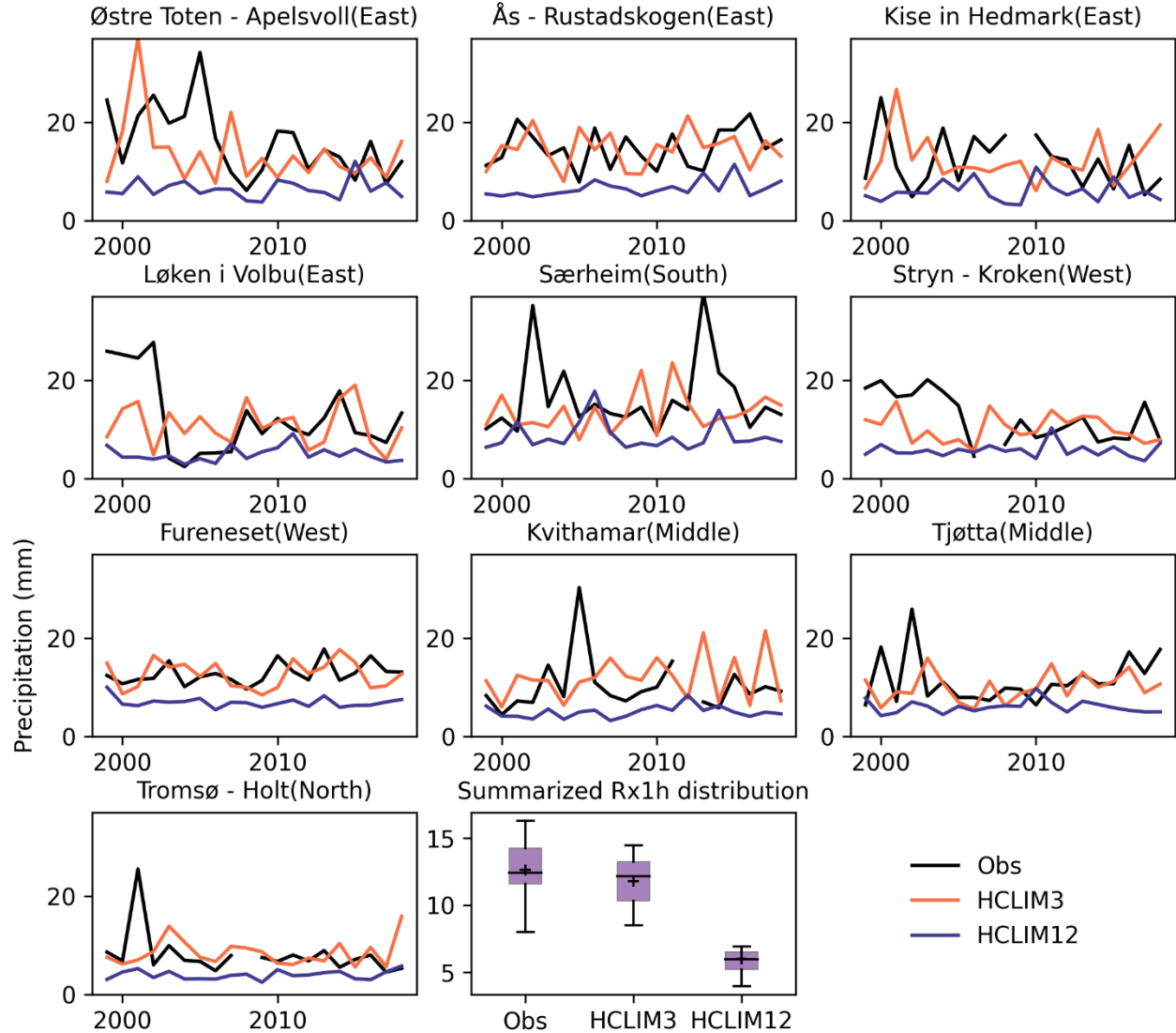
Figure 7: Time evolution of Rx1h precipitation for each year from observation, HCLIM3 and HCLIM12 during 1999-2018 at 10 rain-gauges (Table S1). The final boxplot summarizes the statistical distribution of Rx1h from observations and both HCLIMs simulations.

4.3.2 Return levels

At the local and hourly scale, HCLIM3 has a better representation of hourly extreme events at the 5-, 10-, 20-, and 50-year return periods compared to HCLIM12. Although both HCLIM3 and HCLIM12 tend to underestimate the annual Rx1h for all return periods at almost stations (Fig. 8), the biases between the observations and the interpolated HCLIM3 for all ten rain gauges are consistently lower than those of HCLIM12 for all return periods. The exceptions are Kvithamar (SN69150), Tromsø - Holt (SN90400) and Fureneset (SN56420) which present at all return periods, and Østre Toten - Apelsvoll (SN11500) which present at a 50-year return period, where HCLIM3 slightly overestimation. Notably, the return levels of hourly extreme events at all ten sites are accurately captured by HCLIM3, demonstrating its better ability to capture the extreme hourly precipitation at the 5-, 10-, 20-, and 50-year return periods in localized areas, compared to HCLIM12. This result underscores the added value of CPRCMs in representing hourly extreme precipitation at a very localized scale, despite the overall underestimation of return levels by both HCLIM3 and HCLIM12.

386
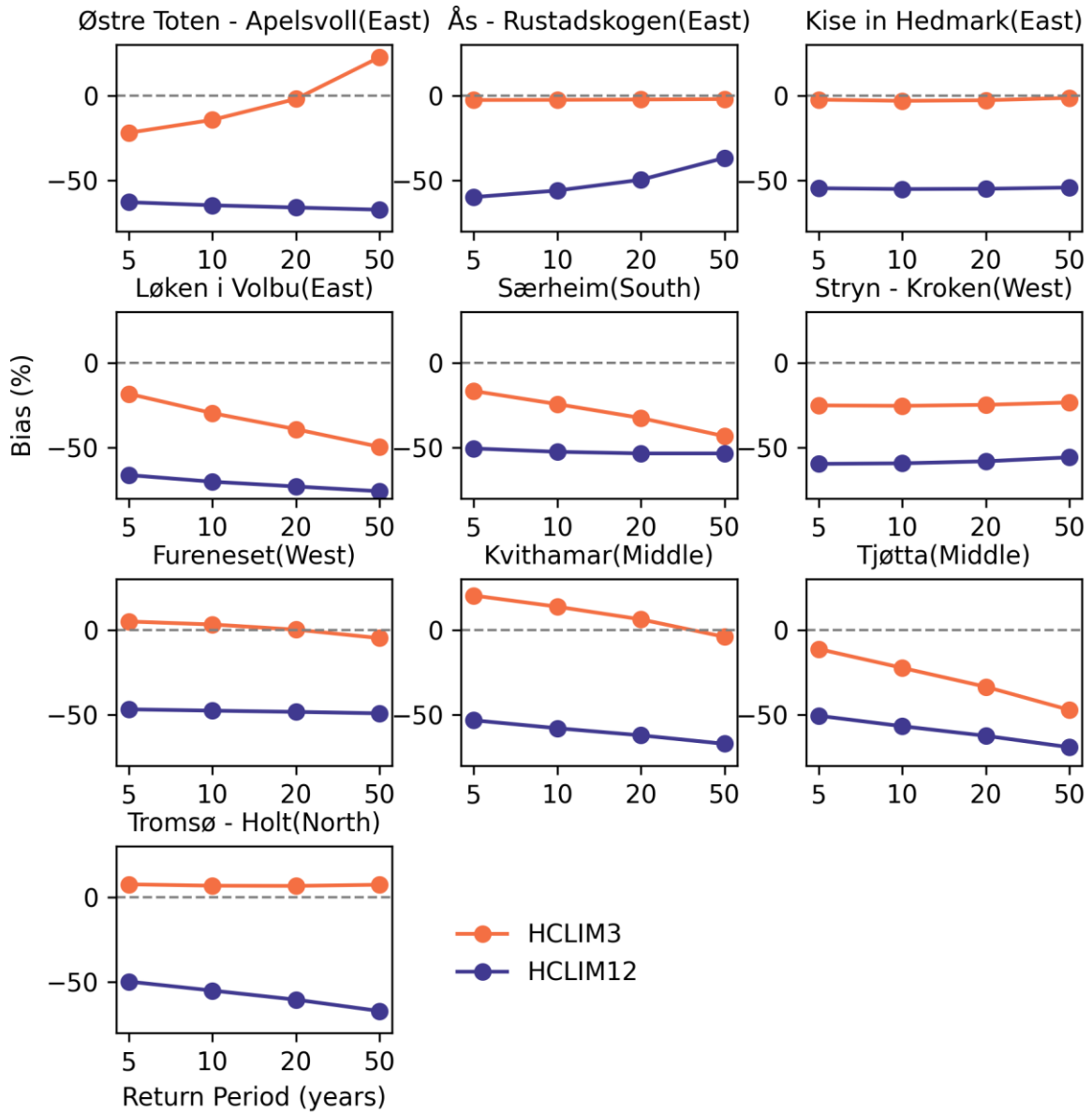
Figure 8: Percentage bias of extreme hourly precipitation exceeding the 5-year to 50-year return periods between HCLIMs (i.e., HCLIM3 and HCLIM12) and in-situ observation in the 10 hourly rain-gauges. Return periods of 5-, 10-, 20-, and 50-year are calculated on the basis of station-scale GEV.

390
391

4.4 Evaluation of seasonality
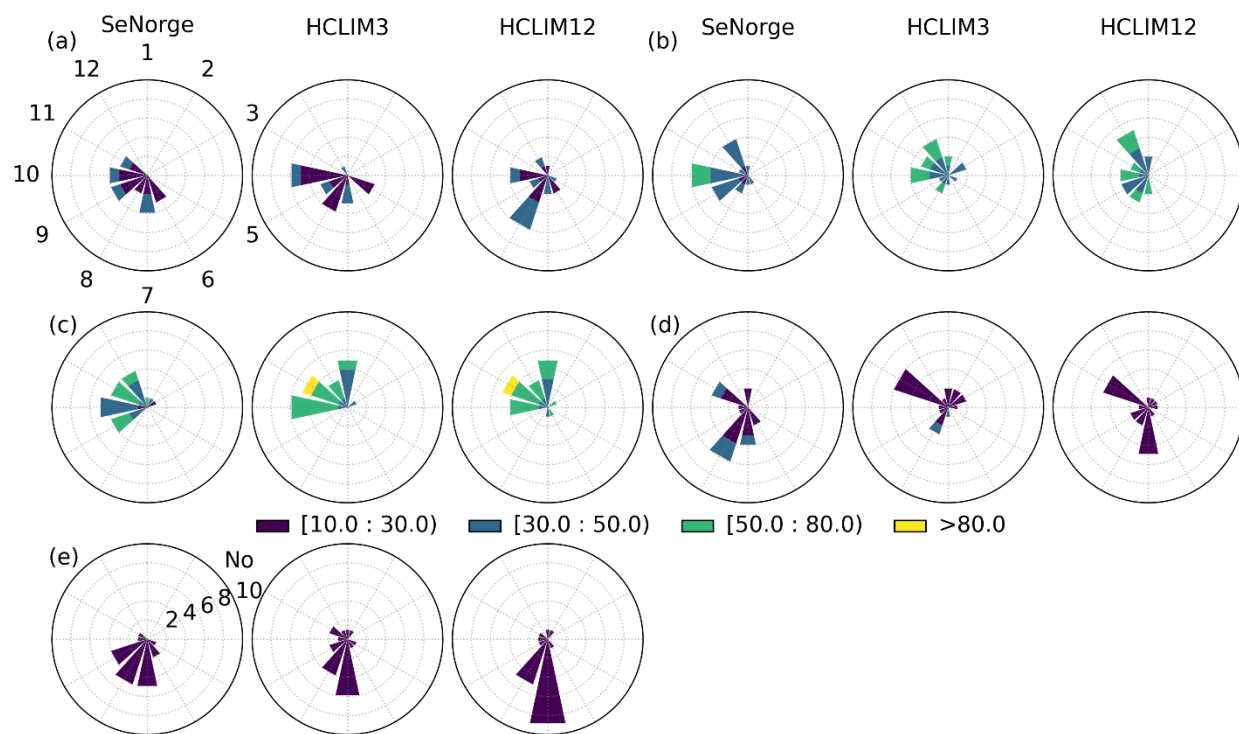
Figure 9: The seasonality of frequency and magnitude of Rx1d precipitation from the SeNorge, HCLIM3 and HCLIM12 during 1999-2018 over different regions: a) East, b) South, c) West, d) Middle, f) North. Radial axis represents the frequency (No). The color represents the magnitude of Rx1d (m³/s). Winter: December, January, February; Spring: March, April, May; Summer: June, July, August; Autumn: September, October, November.

Figure 9 and Figure 10 show the comparison of seasonality (indicated by monthly distribution) of annual Rx1d (e.g., frequency and magnitude) from both HCLIM3 and HCLIM12, compared to SeNorge and in-situ observation, respectively. From the seasonality of observed daily extreme precipitation in Fig. 9, we can see that winter-autumn precipitation dominates in almost east, south and west regions, while in the middle and north regions, spring-summer precipitation is more prevalent. HCLIM3 captures the seasonality of Rx1d frequency at the regional scale in most regions except in middle region, where winter-autumn precipitation dominates. In contrast, HCLIM12 performs poorly in the east and middle regions. It is particularly noteworthy that HCLIM3 has an enhanced ability to capture the seasonality of extreme precipitation frequency over the west region compared to HCLIM12. Heavy precipitation over 50 mm/day occurs mainly in the south and west, which is also simulated by HCLIM3 and HCLIM12. In general, both HCLIM3 and HCLIM12 demonstrate competence in capturing the magnitude of extreme daily precipitation seasonally at regional scale in most regions except middle region. The seasonal performance of Rx1d from HCLIM3 and HCLIM12 in the local scale is also confirmed by the in-situ observation, as shown in Fig. 10. A larger magnitude of annual Rx1d across five regions at local scale than regional scale is shown for observation, HCLIM3 and HCLIM12. Generally, both HCLIM3 and HCLIM12 capture the seasonality of daily extreme precipitation well, HCLIM3 does not consistently shows added value in simulating them.

For the seasonality of annual Rx1d at local scale, as shown in Fig. 11, HCLIM3 more accurately represents the seasonality of Rx1h compared to HCLIM12, which tends to underestimate the frequency of hourly extremes in most

415   sites. Compared with RCMs, CPRCMs demonstrate better potential performance in simulating seasonality of

416   extreme precipitation, with particularly improved accuracy for the hourly extremes at the local scale.

417

418
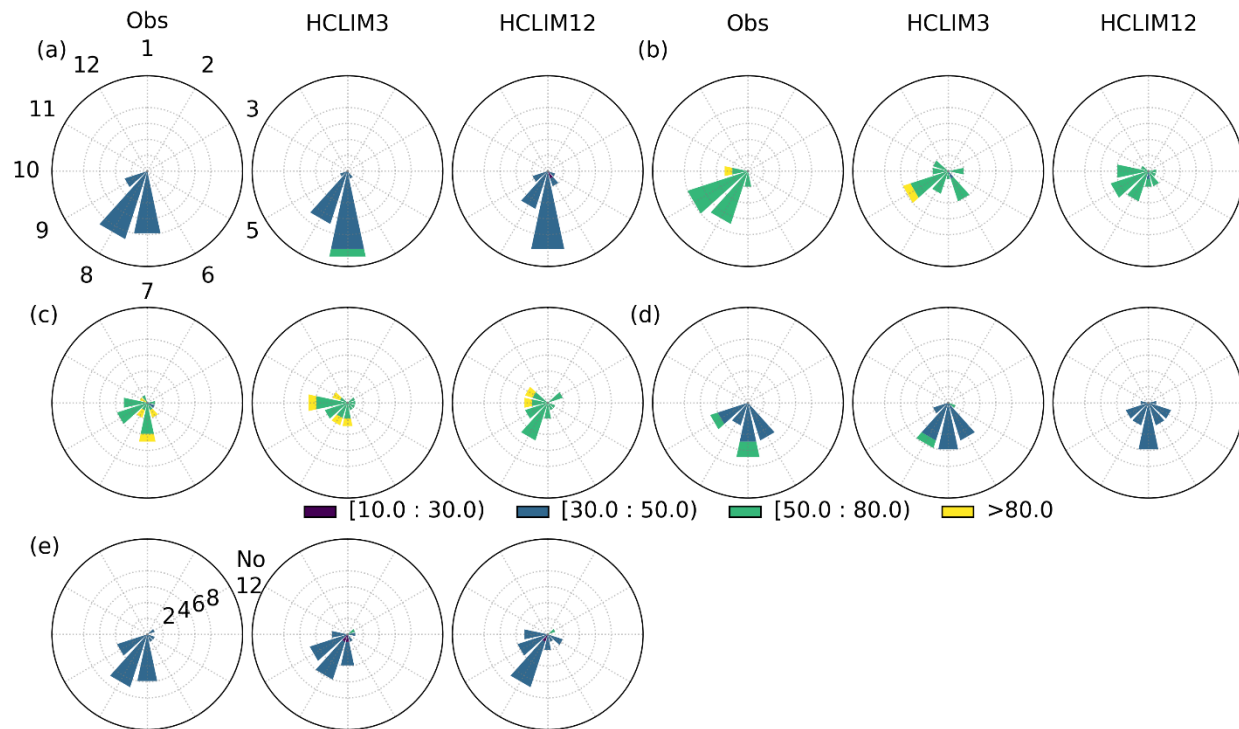
Figure 10: The seasonality of frequency and magnitude of Rx1d precipitation from the in-situ observation, HCLIM3 and
HCLIM12 during 1999-2018 over different regions: a) East, b) South, c) West, d) Middle, f) North. Radial axis represents
the frequency (No). The color represents the magnitude of Rx1d (m³/s).

422
423
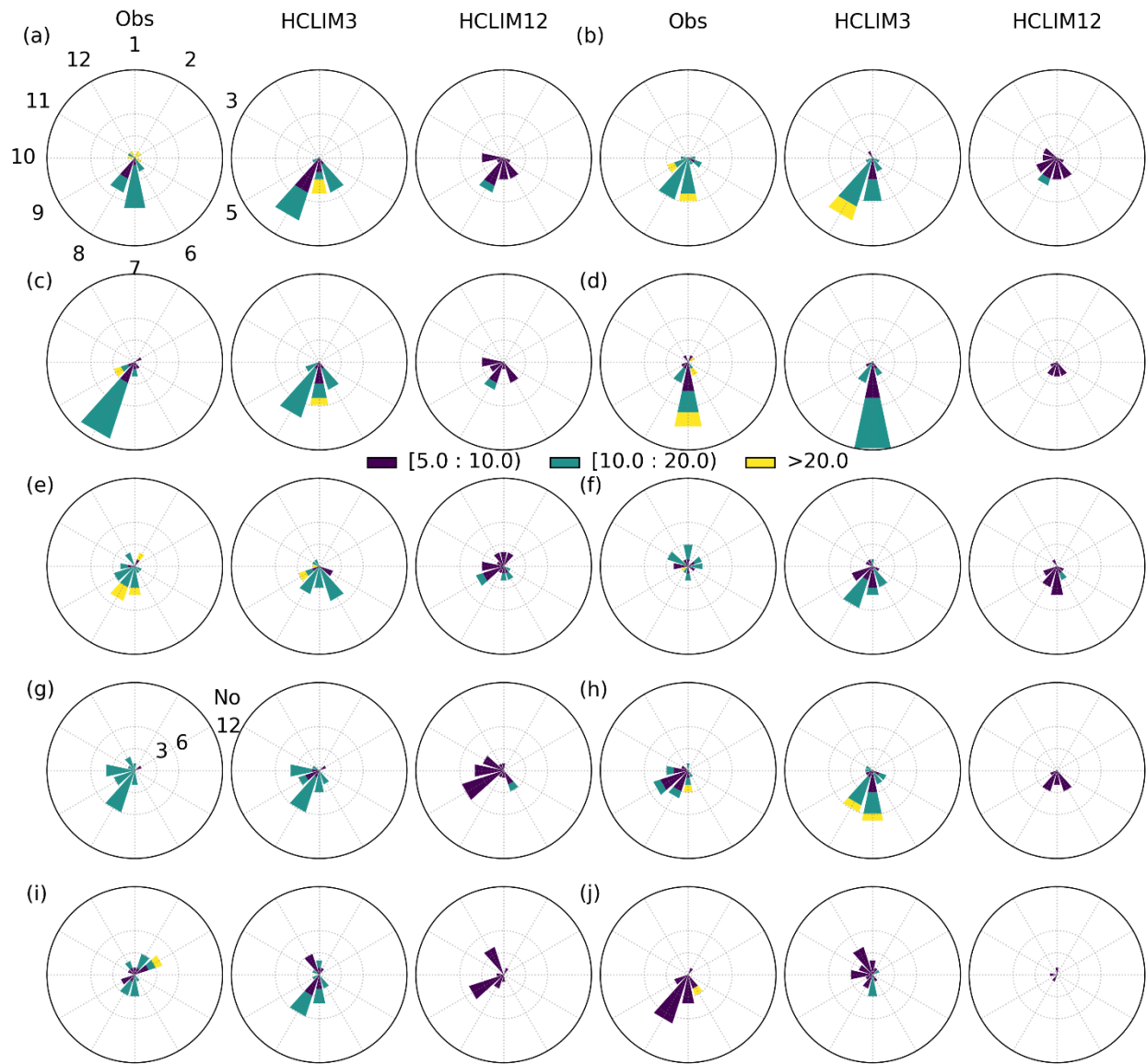
Figure 11: Seasonality of the frequency and magnitude of Rx1h precipitation from the in-situ, HCLIM3 and HCLIM12 during 1999-2018 at 10 rain gauge stations (Table S1), i.e., a) Østre Toten – Apelsvoll (east), b) Ås - Rustadskogen (east), c) Kise in Hedmark (east), d) Løken i Volbu (east), e) Særheim (south), f) Stryn – Kroken (west), g) Fureneset (west) , h) Kvithamar (middle) , i) Tjøtta (middle), j) Tromsø – Holt (north). Radial axis represents the frequency (No). The color represents the magnitude of Rx1h (m³/s).

431 **4.5 Orographic effect on seasonal extreme precipitation**

432 **4.5.1 Seasonal Rx1d at regional scale**
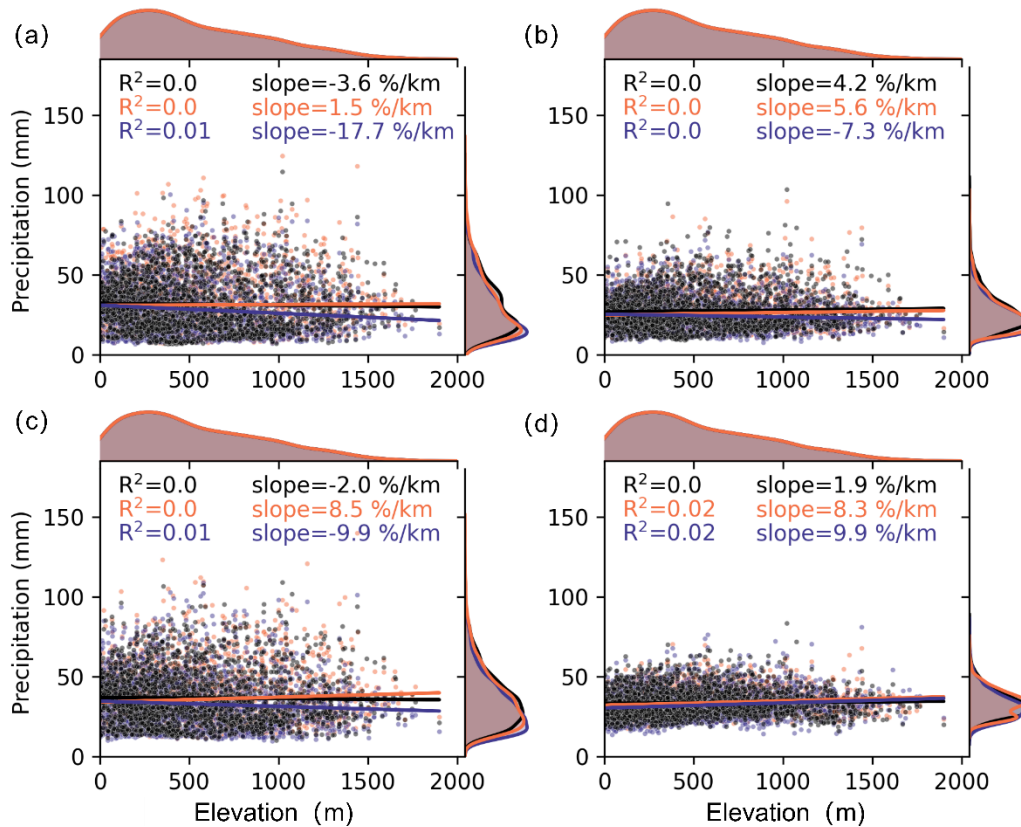
433
434 **Figure 12: Relationship between elevation and Rx1d (maximum 1-day precipitation) for (a) winter, (b) spring, (c)**
435 **summer, and (d) autumn, as derived from SeNorge and HCLIMs (i.e., HCLIM3 and HCLIM12) across mainland Norway**
436 **during the period of 1999-2018.**
437

438 The relationship of seasonal Rx1d with elevation from SeNorge, HCLIM3 and HCLIM12 is shown in Fig. 12.

439 Compared to HCLIM12, HCLIM3 more accurately captures the no evident linear relation (indicated by zero

440 coefficient of determination R^2) of seasonal Rx1d with elevation, similar to SeNorge, though it depicts a more

441 pronounced increase with elevation than SeNorge during summer. For example, both HCLIM3 and HCLIM12

442 simulate a large average increase in summer Rx1d with elevation (over 8 %/km), compared to observation, as

443 indicated by the larger absolute slope values. Generally, SeNorge, HCLIM3 and HCLIM12 showed the weak

444 relationship of seasonal Rx1d with altitude.

445 **4.5.2 Seasonal Rx1d at local scale**

446
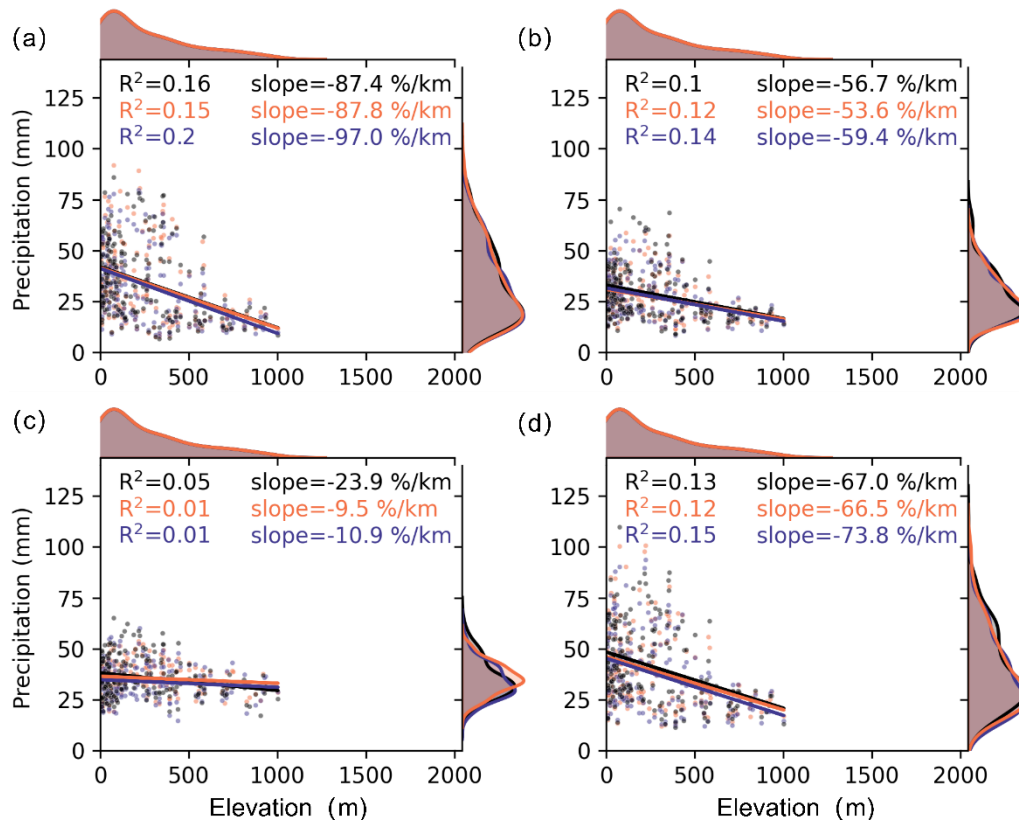
447 **Figure 13: Relationship between elevation and Rx1d (maximum 1-day precipitation) for (a) winter, (b) spring, (c)**
448 **summer, and (d) autumn, based on daily in-situ observation and HCLIMs (i.e., HCLIM3 and HCLIM12) across mainland**
449 **Norway during the period of 1999-2018.**

450

451 Figure 13 represents the relationship of the seasonal Rx1d from in-situ observation, HCLIM3 and HCLIM12 with

452 elevation at local scale. The observed reverse orographic effect, seasonal Rx1d decrease with elevation, clearly

453 depicts with an average decrease of winter, spring, summer and autumn Rx1d of more than 87.4%, 56.7%, 23.9%

454 and 67% per kilometer. HCLIM3 more accurately represents the observed orographic influences on Rx1d in all

455 seasons except summer than HCLIM12. Moreover, HCLIM12 displays a more pronounced decline in Rx1d with

456 elevation, as evidenced by a steeper slope, across all seasons except summer, when compared to observation.

457 Generally, the reverse orographic effect is shown for the Rx1d from in-situ observation, HCLIM3 and HCLIM12.

458   **4.5.3 Seasonal Rx1h at regional scale**

459
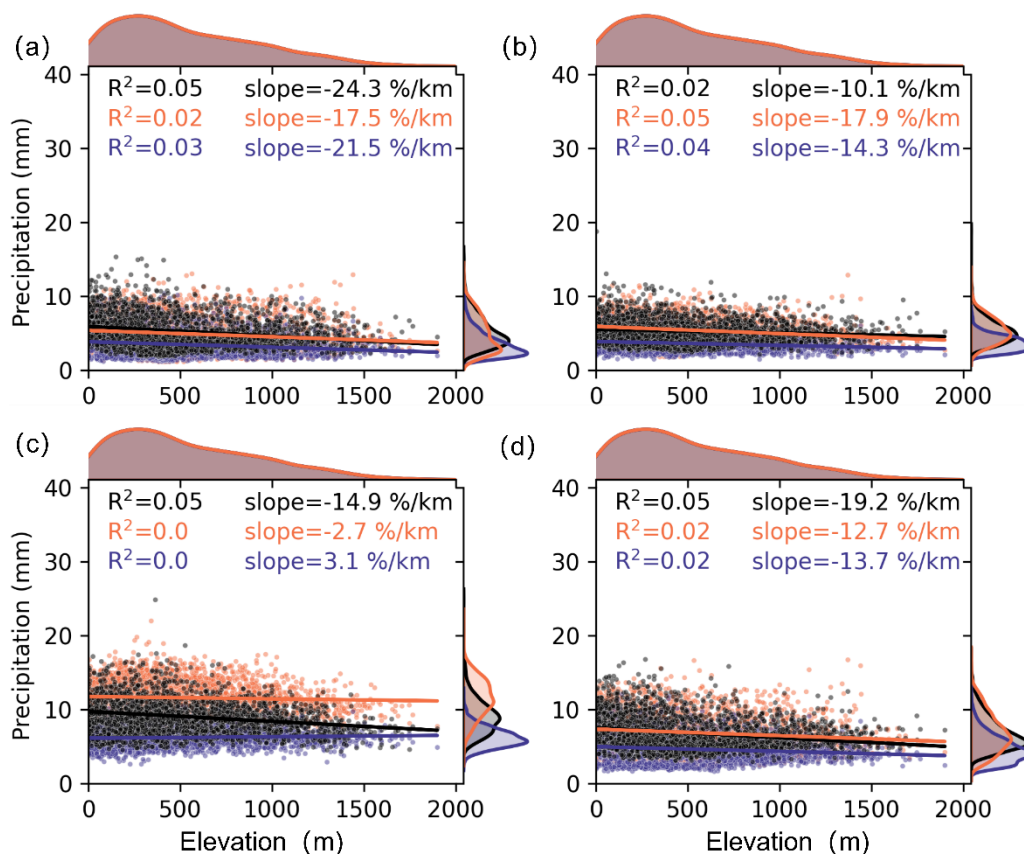
460   **Figure 14: Relationship between elevation and Rx1h (maximum 1-hour precipitation) for (a) winter, (b) spring, (c)**
461   **summer, and (d) autumn, as derived from SeNorge2 and HCLIMs (i.e., HCLIM3 and HCLIM12) across mainland**
462   **Norway during the period of 2010-2018.**

463

464   The relationship of seasonal Rx1h with elevation from gridded observation (SeNorge2) and simulation is further

465   explored, as shown in Fig. 14. The reverse orographic effect of SeNorge2 on Rx1h was manifested in all seasons,

466   with average decreases exceeding 24.3%, 10.1%, 14.9% and 19.2% per kilometer in winter, spring, summer and

467   autumn, respectively. Compared to HCLIM12, HCLIM3 more accurately captures the decrease in seasonal Rx1h

468   with elevation during winter, summer and autumn, though it still underestimates the decrease rate relative to

469   observation. By contrast, HCLIM12 can only reflect the similar reverse orographic on Rx1h with observation in

470   spring. The density plots of Rx1h reveal a dry bias in HCLIM12, particularly noticeable in summer, where it

471   inversely correlates Rx1h with elevation.

472   **5 Discussion**

473   **5.1 Comparison between SeNorge vs in-situ observation**

474
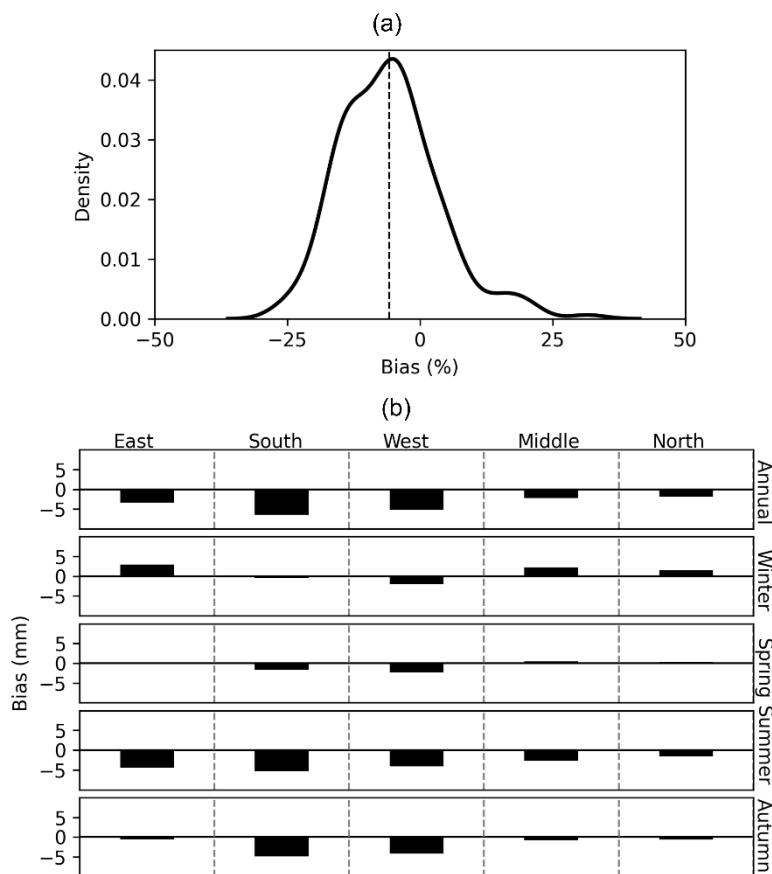
Figure 15: (a) Density distribution of bias for Rx1d between SeNorge and daily in-situ observations from 194 stations during 1999-2018; (b) the percentage difference of seasonal Rx1d between SeNorge and daily in-situ observations across the five regions. The bias is calculated as the SeNorge minus daily in-situ observations at each grid-point.

478

479   To further explore the uncertainty of different observation datasets on local scale model evaluation, we investigate

480   the bias of SeNorge's annual and seasonal Rx1d from daily in-situ observations (see in Fig. 15). Our analysis in the

481   Fig.15 (a) shows that SeNorge mostly underestimates the annual Rx1d compared to in-situ observation at 192

482   stations, with an average bias of -5.8% and a range between -28% and 25%. Although SeNorge data are designed to

483   improve hydrological simulations (Lussana et al., 2019), their dry-biases still persist in most seasons and regions,

484   especially in summer. It is noteworthy that SeNorge slightly overestimates the winter Rx1d in east, middle and north

485   regions. Moreover, SeNorge underestimates the return levels of Rx1d for different return periods (e.g., 5-, 10-, 20-

486   and 50-year) in all regions (Fig. S3).

487   The larger differences between SeNorge and in-situ observation in simulating the Rx1d are manifested in the

488   annual summer and autumn in the south and west, and in the summer in the east, where SeNorge tends to

489   underestimate Rx1d more than in-situ observation. This discrepancy helps explain the differences between

490   HCLIM3's performance in simulating Rx1d in summer in the east and autumn in the south and west at regional

491   scale, compared to the local scale, as shown in Fig. 2 (c) and Fig. 5 (c). Generally, the difference between SeNorge

492   and in-situ observation at daily scale is not very large, which is why in most regions the added value of HCLIM3 in

493 Rx1d at the regional scale is similar to that at the local scale. However, it should be noted that the interpolated

494 precipitation from SeNorge may introduce uncertainties in assessing the performance of CPRCM at the local scale

495 due to the sparse distribution of daily and hourly rain-gauges at high altitude. Especially, for the hourly extremes at

496 the local scale and regional scales, larger uncertainties should be considered due to the limited data from only ten

497 rain-gauges at local scales and nine-years of data series at the regional scale. The impact of station density on the

498 errors of gridded datasets were also highlighted by Gervais et al. (2014b), who suggested that low station density is

499 an important source of errors in such datasets. To address these challenges and enhance the accuracy of extreme

500 precipitation assessments, future studies should prioritize expanding in-situ datasets and improving the spatial

501 coverage of observational networks, especially at the 1-hour timescale.

502 **5.2 Added value of CPRCMs at regional scale**

503 HCLIM3 demonstrates clear advantages over HCLIM12 in capturing the annual Rx1d in most regions. In terms of

504 regional averages, HCLIM12 underestimates Rx1d in most regions except the east and is biased towards wetter,

505 while HCLIM3 shows relatively smaller biases in most regions except the east, due to improvements in

506 microphysics and convection schemes (Lind et al., 2020).

507 Despite the overall better performance of HCLIM3, slightly larger biases in summer over the east, south and

508 west may result from the model's sensitivity to convective processes and limitations in accurately resolving

509 localized dynamics under moisture-rich and unstable atmospheric conditions. These challenges are particularly

510 pronounced during summer, when the intensity of convective activity increases, leading to rapid atmospheric

511 feedbacks and localized extremes (Poujol et al., 2021). In contrast, the south region in winter is mainly affected by

512 atmospheric rivers (ARs) associated to extratropical cyclones, and HCLIM3 can better capture this feature due to its

513 finer resolution.

514 In terms of annual Rx1h, HCLIM3 outperforms HCLIM12, although it exhibits a wet bias compared to

515 SeNorge2. HCLIM12 underestimates Rx1h in most grids, likely due to its reliance on parameterization schemes that

516 fail to capture extremes (Médus et al., 2022). However, HCLIM3 shows larger biases in seasonal Rx1h in the west

517 in all seasons except spring, and in the east and middle region in summer, the overestimation of HCLIM3 over

518 Norway may be attributed to the underestimation in the hourly SeNorge2 (Lussana et al., 2018). Compared with

519 daily extremes, both HCLIM3 and HCLIM12 exhibit larger biases in simulating hourly extremes compared to daily

520 extremes, both at the annual and seasonal scales. It is important to note the limitations of the SeNorge2 dataset,

521 which only spans eight years and is interpolated from sparse hourly rain gauges.

522 In summary, HCLIM3 demonstrates better agreement with observations across most regions of Norway and

523 seasons at the regional scale, with the exception of the east and summer. This is consistent with previous studies

524 highlighting the advantage of convection-permitting models, especially in capturing extreme precipitation events

525 over complex terrain (Kendon et al., 2023; Médus et al., 2022; Lucas-Picher et al., 2021).

5.3 Added value of CPRCMs at local scale

The analysis of local scale convection-permitting climate models (CPRCMs) highlights their better performance in capturing precipitation extremes. HCLIM3 demonstrates notable advantages over HCLIM12, especially in terms of hourly precipitation extremes (Rx1h). For example, HCLIM3 achieves near-zero bias for the annual Rx1d in Norway (Fig. 5) and relative smaller bias for hourly extremes (Fig. 7 and Fig. 8) in all stations, while HCLIM12 consistently underestimates the return levels for hourly extremes at most station (Fig. 8) and daily extremes in all regions. Médus et al. (2022) also pointed out that RCMs underestimate the return levels of Rx1h in Norway. Thomassen et al. (2023) compared the performance of HCLIM3 and HCLIM12 based on local rain-gauge data in Denmark, and found that HCLIM12 indeed underestimate the hourly extreme event and HCLIM3 agree well with observation. Despite these benefits, the added value of HCLIM3 is not uniform across all stations and seasons, which struggle to capture summer daily extremes in the south and west, and the return level in the east and west. However, it should also be noted that the analysis is based on data from only 10 sites, which limits the generalizability of the findings to local hourly extreme events. Further studies of hourly extreme events at more stations are needed to validate these results and provide a more comprehensive understanding. Additionally, the uncertainties in the extreme precipitation analysis based on the stationary GEV method with a 20-years data series should also be noted.

The added value of CPRCMs in simulating hourly precipitation extremes is more obvious at the local scale than at the regional scale. The damped extremes caused by grid-scale averaging may explain the smaller return-level observed for HCLIM3 and HCLIM12 compared to station-level observations. As discussed in Section 5.1, this discrepancy between regional and local scales may be partly due to the inadequate density of in-situ observations.

Few studies have systematically compared hourly and daily rainfall in RCMs due to the challenges in reliably simulating hourly extremes. In line with Ban et al. (2014), we find that RCMs such as HCLIM12 demonstrate reasonably well performance for daily extremes with biases less than 50%. However, CPRCMs such as HCLIM3 perform better for hourly extremes. This is consistent with previous studies (Jiang et al., 2013; Thomassen et al., 2023), such as, Jiang et al. (2013), which showed that it is challenging to capture sub-daily extreme rainfall using RCMs with a resolution of 10 km in the southwest United States. The better performance of CPRCMs compared to RCMs at hourly scale is consistent with the findings by Médus et al. (2022) and Ban et al. (2014), emphasizing that the CPRCMs have significantly better sub-daily precipitation characteristics, including spatial distribution and duration-intensity characteristics. Nonetheless, further improvements in the observation networks and longer observational datasets are necessary to fully verify and realize the benefits of CPRCMs at finer spatial and temporal scales.

Comparison of regional and local extreme precipitation seasonality confirms that HCLIM3 is able to represent the seasonality of daily extremes, although both HCLIM3 and HCLIM12 fail to capture the spring-summer events in the middle region. Moustakis et al. (2021) also highlighted the adequacy of CPRCMs (CTL-WRF~4 km) in capturing seasonality observed over the United States. In particular, we observe HCLIM3 better represent the seasonality of hourly precipitation at the local scale. The persistent underestimation of hourly extremes by

562   HCLIM12 may be attributed to higher uncertainty in its convective parameterization scheme or numerical

563   uncertainties at the local scale.

5.4 Added value of CPRCMs in reproducing reverse orographic effect

565   An unclear relation of daily extreme precipitation with elevation was also seen from the study of Dallan et al.

566   (2023), in which they analyzed annual daily return level based on CPRCMs and in-situ observation over an Alpine

567   region. By comparing the relationship between elevation and seasonal variation of extreme precipitation, HCLIM3

568   represents the reverse orographic effect well at regional and local scale, although there is a weak relationship

569   between extreme precipitation and elevation at the regional scale. The reverse orographic effects on hourly and daily

570   extremes vary with seasons, indicating the influence of topography on extreme precipitation at different timescales

571   and emphasizing the reliability of simulation of extreme precipitation over complex terrain. Unlike Rx1d at the

572   regional scale, which is less affected by topography, the slope of the reverse orographic effect of daily extreme

573   precipitation at the local scale is more clearly. From a seasonal perspective, the reverse orographic effect of extreme

574   precipitation in summer is not well captured in HCLIM3 and HCLIM12, which may be related to the intense

575   orographically-sustained convection affected by the atmospheric, aerosol conditions, local terrain slope and

576   shadowing effects, which RCMs and CPRCMs fail to capture (Dallan et al., 2023; Poujol et al., 2021).

577   For hourly extremes, the reverse orography effect of seasonal Rx1h in this study is consistent with the reverse

578   orographic effect of hourly return level, as found by Dallan et al. (2023) over the Alpine region. HCLIM3 and

579   HCLIM12 well capture the reverse orography effect on seasonal Rx1h, especially in HCLIM3, although a stronger

580   decrease of Rx1h with elevation is observed from SeNorge2 except spring. In comparison, lower Rx1h and weak

581   reverse orography effect is found in HCLIM12 in all seasons. Our findings confirm the reverse orographic effect on

582   Rx1h, as demonstrated by Marra et al. (2021) for hourly precipitation and Formetta et al. (2022) for sub-hourly

583   scale.

584   Furthermore, we demonstrate the reverse orographic effect for both seasonal Rx1h and Rx1d, which contrasts

585   with the findings of Formetta et al. (2022), who identified an orographic enhancement for durations of

586   approximately 8 hours or longer, although a reverse orographic effect for hourly and sub-hourly durations was

587   shown. These difference, which may be attributed to the combined effects of latitude, climate, altitude zones, static

588   atmospheric or aerosol conditions, and shadowing effects (Amponsah et al., 2022; Napoli et al., 2019).

589   It should be noted that simple relationship between extreme precipitation and elevation is difficult to build due

590   to several land surface characteristics could influence the precipitation, a complex regression model should be

591   considered to more realistically quantify the reverse orographic effect (Zhang et al., 2018) in the future. The

592   interpolated gridded dataset and limited rain gauges over the complex orography, along with the decreasing station

593   density at higher elevations, may also limit the reliable analysis of the reverse orographic effect. The sparsity of rain

594   gauges and under catch problems could also lead to underestimation of precipitation, especially in the complex

595   orography (Lussana et al., 2018, 2019; Gervais et al., 2014b).

6 Conclusions

597 In this study, we conducted a comprehensive evaluation of extreme precipitation characteristics from regional to
598 local scale in Norway, focusing on five distinct regions, utilizing a convection-permitting regional climate model
599 (HCLIM3) and comparing it with its convection-parameterized regional climate model (HCLIM12) forced by ERA-
600 Interim data during 1999-2018.

601   The key conclusions of this study are as follows:

602 a) At regional scale, HCLIM3 general performs better than HCLIM12 in capturing Rx1d across most regions
603   and seasons, except for larger biases in summer over the east, south, and west, as well as in the return
604   levels of daily extremes in the east. In contrast, HCLIM12 consistent underestimates the annual daily
605   extremes in all regions except the east. For hourly extremes, HCLIM3 outperforms HCLIM12 in most
606   regions and seasons except in summer and over the west. In general, HCLIM3 overestimates annual Rx1h
607   across most grid points in Norway, while HCLIM12 underestimates it.

608 b) At local scale, HCLIM3 also shows added value compared to HCLIM12 in capturing Rx1d in most
609   regions and seasons. Specifically, HCLIM3 can better capture the return levels of daily extremes in most
610   regions except in the west and east, and it shows smaller biases in Rx1d across Norway for all seasons,
611   except summer in the south and west. Overall, HCLIM3 shows consistent benefit in capturing the daily
612   extremes in the middle and north regions compared with HCLIM12, both at the regional and local scales.
613   For hourly extremes, HCLIM3 outperforms HCLIM12 in capturing the annual Rx1h and return levels in
614   those 10 stations.

615 c) For the seasonality of extremes, HCLIM3 and HCLIM12 can well characterize the seasonality of daily
616   extremes in most regions. A distinct advantage emerges with HCLIM3 for hourly extremes, where it
617   accurately reflects both the occurrence and intensity of these events across different seasons, while
618   HCLIM12 tends to underestimate these aspects.

619 d) In Norway, the effect of the preserved topography on seasonal Rx1h and Rx1d emerge from regional to
620   local scales, although weak relationship between Rx1d and elevation is demonstrated at regional scale. For
621   seasonal Rx1h, both HCLIM3 and HCLIM12 can capture the reverse orographic effect at regional scale,
622   but no added value is shown in HCLIM3. At the local scale, HCLIM3 provides added value in capturing
623   the reverse orographic effect of seasonal Rx1d in all seasons except summer.

Data availability

625 All simulation data in this paper are available from the authors upon request (luli@norceresearch.no).

Author contribution

627 KX and LL initiated and designed the study. KX further refined the idea and was primarily responsible for the
628 modeling, analysis, and drafting as well as revising the manuscript. LL contributed to data collection, writing and
629 reviewing the manuscript. HC contributed to the manuscript review. AD assisted in collecting regional climate
630 model datasets and contributed to the manuscript review. CYX, SM, and OMG contributed to the manuscript
631 review.

632 **Competing interests**

633 The authors declare that they have no conflict of interest.

634 **Acknowledgments**

635 We would like to thank Stefan P. Sobolowski, for his great support as PI of the EU Impetus4change (I4C) project.

636 The computer resources where available through the RCN's program for supercomputing (NOTUR/NORSTORE);

637 projects NN10014K and NS10014K. This work uses data from the NorCP project, which is a Nordic collaboration

638 involving climate modeling groups from the Danish Meteorological Institute (DMI), Finnish Meteorological

639 Institute (FMI), Norwegian Meteorological Institute (MET Norway) and the Swedish Meteorological and

640 Hydrological Institute (SMHI).

641 **Financial support**

642 This research was supported by the European Union's Horizon 2020 research, innovation programme under grant

643 agreement no. 101081555 (IMPETUS4CHANGE) and the Research Council of Norway through FRINATEK

644 Project 274310.

645

646 **References**

647 Adinolfi, M., Raffa, M., Reder, A., and Mercogliano, P.: Evaluation and Expected Changes of Summer Precipitation
648   at Convection Permitting Scale with COSMO-CLM over Alpine Space, 10.3390/atmos12010054, 2021.

649 Amponsah, W., Dallan, E., Nikolopoulos, E. I., and Marra, F.: Climatic and altitudinal controls on rainfall extremes
650   and their temporal changes in data-sparse tropical regions. Journal of Hydrology 612, 128090.
651   https://doi.org/10.1016/j.jhydrol.2022.128090, 2022.

652 Ban, N., Schmidli, J., and Schär, C.: Evaluation of the convection-resolving regional climate modeling approach in
653   decade-long simulations, Journal of Geophysical Research: Atmospheres, 119, 7889-7907,
654   https://doi.org/10.1002/2014JD021478, 2014.

655 Ban, N., Rajczak, J., Schmidli, J., and Schär, C.: Analysis of Alpine precipitation extremes using generalized
656   extreme value theory in convection-resolving climate simulations, Climate Dynamics, 55, 61-75,
657   10.1007/s00382-018-4339-4, 2020.

658 Belušić, D., de Vries, H., Dobler, A., Landgren, O., Lind, P., Lindstedt, D., Pedersen, R. A., Sánchez-Perrino, J. C.,
659   Toivonen, E., van Ulft, B., Wang, F., Andrae, U., Batrak, Y., Kjellström, E., Lenderink, G., Nikulin, G.,
660   Pietikäinen, J.-P., Rodríguez-Camino, E., Samuelsson, P., van Meijgaard, E., and Wu, M.: HCLIM38: a
661   flexible regional climate model applicable for different climate zones from coarse to convection-permitting
662   scales, Geosci. Model Dev., 13, 1311–1333, 10.5194/gmd-13-1311-2020, 2020.

663 Chapman, S., Bacon, J., Birch, C. E., Pope, E., Marsham, J. H., Msemo, H., Nkonde, E., Sinachikupo, K., and
664   Vanya, C.: Climate Change Impacts on Extreme Rainfall in Eastern Africa in a Convection-Permitting
665   Climate Model, Journal of Climate, 36, 93-109, https://doi.org/10.1175/JCLI-D-21-0851.1, 2023.

Coles, S., Pericchi, L. R., and Sisson, S.: A fully probabilistic approach to extreme rainfall modeling, Journal of Hydrology, 273, 35-50, https://doi.org/10.1016/S0022-1694(02)00353-0, 2003.

Dallan, E., Marra, F., Fosser, G., Marani, M., Formetta, G., Schär, C., and Borga, M.: How well does a convection-permitting regional climate model represent the reverse orographic effect of extreme hourly precipitation?, Hydrol. Earth Syst. Sci., 27, 1133-1149, 10.5194/hess-27-1133-2023, 2023.

Di Piazza, A., Conti, F. L., Noto, L. V., Viola, F., and La Loggia, G.: Comparative analysis of different techniques for spatial interpolation of rainfall data to create a serially complete monthly time series of precipitation for Sicily, Italy, International Journal of Applied Earth Observation and Geoinformation, 13, 396-408, https://doi.org/10.1016/j.jag.2011.01.005, 2011.

Dyrrdal, A. V., Médus, E., Dobler, A., Hodnebrog, Ø., Arnbjerg-Nielsen, K., Olsson, J., Thomassen, E. D., Lind, P., Gaile, D., and Post, P.: Changes in design precipitation over the Nordic-Baltic region as given by convection-permitting climate simulations, Weather and Climate Extremes, 42, 100604, 10.1016/j.wace.2023.100604, 2023.

Formetta, G., Marra, F., Dallan, E., Zaramella, M., and Borga, M.: Differential orographic impact on sub-hourly, hourly, and daily extreme precipitation. Advances in Water Resources 159, 104085. https://doi.org/10.1016/j.advwatres.2021.104085, 2022.

Gervais, M., Gyakum, J. R., Atallah, E., Tremblay, L. B., and Neale, R. B.: How Well Are the Distribution and Extreme Values of Daily Precipitation over North America Represented in the Community Climate System Model? A Comparison to Reanalysis, Satellite, and Gridded Station Data, Journal of Climate, 27, 5219-5239, https://doi.org/10.1175/JCLI-D-13-00320.1, 2014a.

Gervais, M., Tremblay, L. B., Gyakum, J. R., and Atallah, E.: Representing Extremes in a Daily Gridded Precipitation Analysis over the United States: Impacts of Station Density, Resolution, and Gridding Methods, Journal of Climate, 27, 5201-5218, https://doi.org/10.1175/JCLI-D-13-00319.1, 2014b.

Giordani, A., Cerenzia, I. M. L., Paccagnella, T., and Di Sabatino, S.: SPHERA, a new convection-permitting regional reanalysis over Italy: Improving the description of heavy rainfall, Quarterly Journal of the Royal Meteorological Society, 149, 781-808, https://doi.org/10.1002/qj.4428, 2023.

Jiang, P., Gautam, M. R., Zhu, J., and Yu, Z.: How well do the GCMs/RCMs capture the multi-scale temporal variability of precipitation in the Southwestern United States?, Journal of Hydrology, 479, 75-85, https://doi.org/10.1016/j.jhydrol.2012.11.041, 2013.

Kendon, E. J., Fischer, E. M., and Short, C. J.: Variability conceals emerging trend in 100yr projections of UK local hourly rainfall extremes, Nature Communications, 14, 1133, 10.1038/s41467-023-36499-9, 2023.

Kendon, E. J., Stratton, R. A., Tucker, S., Marsham, J. H., Berthou, S., Rowell, D. P., and Senior, C. A.: Enhanced future changes in wet and dry extremes over Africa at convection-permitting scale, Nature Communications, 10, 1794, 10.1038/s41467-019-09776-9, 2019.

Kent, C., Dunstone, N., Tucker, S., Scaife, A. A., Brown, S., Kendon, E. J., Smith, D., McLean, L., and Greenwood, S.: Estimating unprecedented extremes in UK summer daily rainfall, Environmental Research Letters, 17, 014041, 10.1088/1748-9326/ac42fb, 2022.

Kim, Y., Rocheta, E., Evans, J. P., and Sharma, A.: Impact of bias correction of regional climate model boundary conditions on the simulation of precipitation extremes, Climate Dynamics, 55, 3507-3526, 10.1007/s00382-020-05462-5, 2020.

Knist, S., Goergen, K., and Simmer, C.: Evaluation and projected changes of precipitation statistics in convection-permitting WRF climate simulations over Central Europe, Climate Dynamics, 55, 325-341, 10.1007/s00382-018-4147-x, 2020.

Konstali, K. and Sorteberg, A.: Why has Precipitation Increased in the Last 120 Years in Norway?, Journal of Geophysical Research: Atmospheres, 127, 10.1029/2021jd036234, 2022.

Li, J., Gan, T. Y., Chen, Y. D., Gu, X., Hu, Z., Zhou, Q., and Lai, Y.: Tackling resolution mismatch of precipitation extremes from gridded GCMs and site-scale observations: Implication to assessment and future projection, Atmospheric Research, 239, 104908, https://doi.org/10.1016/j.atmosres.2020.104908, 2020a.

Li, L., Pontoppidan, M., Sobolowski, S., and Senatore, A.: The impact of initial conditions on convection-permitting simulations of a flood event over complex mountainous terrain, Hydrol. Earth Syst. Sci., 24, 771-791, 10.5194/hess-24-771-2020, 2020b.

Li, P., Furtado, K., Zhou, T., Chen, H., and Li, J.: Convection-permitting modelling improves simulated precipitation over the central and eastern Tibetan Plateau, Quarterly Journal of the Royal Meteorological Society, 147, 341-362, https://doi.org/10.1002/qj.3921, 2021.

Lind, P., Lindstedt, D., Kjellström, E., and Jones, C.: Spatial and Temporal Characteristics of Summer Precipitation over Central Europe in a Suite of High-Resolution Climate Models, Journal of Climate, 29, 3501-3518, https://doi.org/10.1175/JCLI-D-15-0463.1, 2016.

Lind, P., Belušić, D., Christensen, O. B., Dobler, A., Kjellström, E., Landgren, O., Lindstedt, D., Matte, D., Pedersen, R. A., Toivonen, E., and Wang, F.: Benefits and added value of convection-permitting climate modeling over Fenno-Scandinavia, Climate Dynamics, 55, 1893-1912, 10.1007/s00382-020-05359-3, 2020.

Liu, C., Ikeda, K., Rasmussen, R., Barlage, M., Newman, A. J., Prein, A. F., Chen, F., Chen, L., Clark, M., Dai, A., Dudhia, J., Eidhammer, T., Gochis, D., Gutmann, E., Kurkute, S., Li, Y., Thompson, G., and Yates, D.: Continental-scale convection-permitting modeling of the current and future climate of North America, Climate Dynamics, 49, 71-95, 10.1007/s00382-016-3327-9, 2017.

Lucas-Picher, P., Argüeso, D., Brisson, E., Tramblay, Y., Berg, P., Lemonsu, A., Kotlarski, S., and Caillaud, C.: Convection-permitting modeling with regional climate models: Latest developments and next steps. WIREs Climate Change 12(6), e731. https://doi.org/10.1002/wcc.731, 2021.

Lussana, C., Tveito, O. E., Dobler, A., and Tunheim, K.: seNorge_2018, daily precipitation, and temperature datasets over Norway, Earth Syst. Sci. Data, 11, 1531-1551, 10.5194/essd-11-1531-2019, 2019.

Lussana, C., Saloranta, T., Skaugen, T., Magnusson, J., Tveito, O. E., and Andersen, J.: seNorge2 daily precipitation, an observational gridded dataset over Norway from 1957 to the present day, Earth Syst. Sci. Data, 10, 235-249, 10.5194/essd-10-235-2018, 2018.

739 Mahoney, K., Ralph, F. M., Wolter, K., Doesken, N., Dettinger, M., Gottas, D., Coleman, T., and White, A.:
740   Climatology of Extreme Daily Precipitation in Colorado and Its Diverse Spatial and Seasonal Variability,
741   Journal of Hydrometeorology, 16, 781-792, https://doi.org/10.1175/JHM-D-14-0112.1, 2015.

742 Marra, F., Armon, M., Borga, M., and Morin, E.: Orographic Effect on Extreme Precipitation Statistics Peaks at
743   Hourly Time Scales, Geophysical Research Letters, 48, e2020GL091498,
744   https://doi.org/10.1029/2020GL091498, 2021.

745 Médus, E., Thomassen, E. D., Belušić, D., Lind, P., Berg, P., Christensen, J. H., Christensen, O. B., Dobler, A.,
746   Kjellström, E., Olsson, J., and Yang, W.: Characteristics of precipitation extremes over the Nordic region:
747   added value of convection-permitting modeling, Nat. Hazards Earth Syst. Sci., 22, 693-711, 10.5194/nhess-
748   22-693-2022, 2022.

749 Michel, C., Sorteberg, A., Eckhardt, S., Weijenborg, C., Stohl, A., and Cassiani, M.: Characterization of the
750   atmospheric environment during extreme precipitation events associated with atmospheric rivers in Norway
751   - Seasonal and regional aspects, Weather and Climate Extremes, 34, 100370, 10.1016/j.wace.2021.100370,
752   2021.

753 Moustakis, Y., Papalexiou, S. M., Onof, C. J., and Paschalis, A.: Seasonality, Intensity, and Duration of Rainfall
754   Extremes Change in a Warmer Climate, Earth's Future, 9, e2020EF001824,
755   https://doi.org/10.1029/2020EF001824, 2021.

756 Napoli, A., Crespi, A., Ragone, F., Maugeri, M., and Pasquero, C.: Variability of orographic enhancement of
757   precipitation in the Alpine region. Scientific Reports 9(1), 13352. 10.1038/s41598-019-49974-5, 2019.

758 Piani, C., Weedon, G. P., Best, M., Gomes, S. M., Viterbo, P., Hagemann, S., and Haerter, J. O.: Statistical bias
759   correction of global simulated daily precipitation and temperature for the application of hydrological
760   models, Journal of Hydrology, 395, 199-215, https://doi.org/10.1016/j.jhydrol.2010.10.024, 2010.

761 Pontoppidan, M., Kolstad, E. W., Sobolowski, S., and King, M. P.: Improving the Reliability and Added Value of
762   Dynamical Downscaling via Correction of Large-Scale Errors: A Norwegian Perspective, Journal of
763   Geophysical Research: Atmospheres, 123, 11,875-811,888, 10.1029/2018jd028372, 2018.

764 Poujol, B., Mooney, P. A., and Sobolowski, S. P.: Physical processes driving intensification of future precipitation
765   in the mid- to high latitudes, Environmental Research Letters, 16, 034051, 10.1088/1748-9326/abdd5b,
766   2021.

767 Prein, A. F., Langhans, W., Fosser, G., Ferrone, A., Ban, N., Goergen, K., Keller, M., Tölle, M., Gutjahr, O., Feser,
768   F., Brisson, E., Kollet, S., Schmidli, J., van Lipzig, N. P. M., and Leung, R.: A review on regional
769   convection-permitting climate modeling: Demonstrations, prospects, and challenges, Reviews of
770   Geophysics, 53, 323-361, https://doi.org/10.1002/2014RG000475, 2015.

771 Reder, A., Raffa, M., Montesarchio, M., and Mercogliano, P.: Performance evaluation of regional climate model
772   simulations at different spatial and temporal scales over the complex orography area of the Alpine region,
773   Natural Hazards, 102, 151-177, 10.1007/s11069-020-03916-x, 2020.

774   Rossi, M. W., Anderson, R. S., Anderson, S. P., and Tucker, G. E.: Orographic Controls on Subdaily Rainfall
775   Statistics and Flood Frequency in the Colorado Front Range, USA, Geophysical Research Letters, 47,
776   e2019GL085086, https://doi.org/10.1029/2019GL085086, 2020.

777   Tabari, H.: Climate change impact on flood and extreme precipitation increases with water availability, Scientific
778   Reports, 10, 13768, 10.1038/s41598-020-70816-2, 2020.

779   Thackeray, C. W., Hall, A., Norris, J., and Chen, D.: Constraining the increased frequency of global precipitation
780   extremes under warming, Nature Climate Change, 12, 441-448, 10.1038/s41558-022-01329-1, 2022.

781   Thomassen, E. D., Arnbjerg-Nielsen, K., Sørup, H. J. D., Langen, P. L., Olsson, J., Pedersen, R. A., and
782   Christensen, O. B.: Spatial and temporal characteristics of extreme rainfall: Added benefits with sub-
783   kilometre-resolution climate model simulations?, Quarterly Journal of the Royal Meteorological Society,
784   149, 1913-1931, https://doi.org/10.1002/qj.4488, 2023.

785   Wang, Y., Zhang, G. J., and He, Y.-J.: Simulation of Precipitation Extremes Using a Stochastic Convective
786   Parameterization in the NCAR CAM5 Under Different Resolutions, Journal of Geophysical Research:
787   Atmospheres, 122, 12,875-812,891, https://doi.org/10.1002/2017JD026901, 2017.

788   Zhang, T., Li, B., Yuan, Y., Gao, X., Sun, Q., Xu, L., and Jiang, Y.: Spatial downscaling of TRMM precipitation
789   data considering the impacts of macro-geographical factors and local elevation in the Three-River
790   Headwaters Region, Remote Sensing of Environment, 215, 109-127,
791   https://doi.org/10.1016/j.rse.2018.06.004, 2018.

792   Vormoor, K., Lawrence, D., Schlichting, L., Wilson, D., and Wong, W. K.: Evidence for changes in the magnitude
793   and frequency of observed rainfall vs. snowmelt driven floods in Norway, Journal of Hydrology, 538, 33-
794   48, 10.1016/j.jhydrol.2016.03.066, 2016.

795   Whan, K., Sillmann, J., Schaller, N., and Haarsma, R.: Future changes in atmospheric rivers and extreme
796   precipitation in Norway. Climate Dynamics 54(3), 2071-2084. 10.1007/s00382-019-05099-z, 2020.